

Quasi-symmetry Constrained Spin Ferromagnetism in Altermagnets

Mercè Roig,^{1,2} Yue Yu,² Rune C. Ekman,¹ Andreas Kreisel,¹ Brian M. Andersen,¹ and Daniel F. Agterberg²

¹*Niels Bohr Institute, University of Copenhagen, DK-2100 Copenhagen, Denmark*

²*Department of Physics, University of Wisconsin-Milwaukee, Milwaukee, Wisconsin 53201, USA*

Altermagnets break time-reversal symmetry and their spin-orbit coupling (SOC) allow for an anomalous Hall effect (AHE) that depends on the direction of the Néel ordering vector. The AHE and the ferromagnetic spin moment share the same symmetry and hence are usually proportional. However, density functional theory (DFT) calculations find that the AHE exists with negligible ferromagnetic spin moment for some compounds, whereas it reaches sizable values for other altermagnets. By examining realistic minimal models for altermagnetism in which the DFT phenomenology is captured, we uncover a general SOC-enabled quasi-symmetry, the uniaxial spin space-group, that provides a natural explanation for the amplitude of the ferromagnetic spin moment across the vast range of different altermagnetic materials. Additionally, we derive analytic expressions for the magnetic anisotropy energy, providing a simple means to identify the preferred Néel vector orientation for altermagnets.

Introduction.— The Hall effect has been a frontier theme in condensed matter physics for more than half a century. Fundamental understanding of the quantized Hall conductance and the anomalous Hall effect (AHE) has helped pave the way for topological classifications of quantum matter and the importance of Berry curvature in transport properties [1–7]. The discovery of altermagnetism (AM) and its associated large antiferromagnetic AHE is yet another testimony to this development [8–17], which may open new opportunities for devices utilizing dissipationless transport and spintronics technologies [5, 18–22].

The AHE in AM, which we describe here as an intra-unit cell Néel order, is only nonzero for certain directions of the Néel vector and in the presence of relativistic spin-orbit coupling (SOC). This, in addition, induces weak ferromagnetism (FM), which satisfies the same symmetry properties as the AHE [23, 24]. This implies that, in principle, FM and AHE share the same dependence on the orientation of the Néel vector [21, 25, 26]. However, from DFT it is found that the relative amplitude of the AHE transport coefficient and the FM spin moment depends strongly on the particular AM material under investigation. For example, for RuO₂ and MnTe, DFT finds a large AHE of 40 S/cm and 300 S/cm, respectively, while RuO₂ has a nearly zero FM moment (that we estimate is of the order $10^{-7} \mu_B$) and Mn in MnTe has $10^{-4} \mu_B$ [17, 18, 27]. In the case of MnTe and RuO₂, weak FM was also reported experimentally [16, 28], though the AM ground state of the latter material is still debated [29, 30]. A weak FM spin moment has also been identified by DFT in CrSb [31]. By contrast, in other AM, such as FeSb₂, DFT finds a large AHE of 143 S/cm [32, 33], and our calculations estimate a moderate FM moment of $0.03 \mu_B$. Similarly, the material RuF₄ has also been predicted by DFT to exhibit a large FM spin moment of $0.22 \mu_B$ on the Ru sites [34]. These results suggest that while the AHE is generically large when allowed by symmetry, the corresponding FM moment is

strongly dependent on the AM state and this is poorly understood.

To gain deeper insight into the interplay between the AHE, the FM moment, and the AM state it is crucial to analyze the role of SOC using realistic models. Here, by examining realistic microscopic models for AM in which the DFT phenomenology is captured [35], we identify which AM states have a large SOC induced AHE but a small FM spin moment and find good agreement with DFT results. In addition, we find that our model-based results are more generally valid. Specifically, they apply to all microscopic theories in which AM appears as a consequence of the exchange interaction. To show this, we identify a general SOC-enabled quasi-symmetry [36, 37], a uniaxial spin-space group, that establishes for which AM symmetries the symmetry-allowed FM is large or vanishingly small. Finally, the presence of SOC in AM breaks the spin-space degeneracy and leads to a preferred direction for the Néel vector. For example, DFT calculations have revealed that the moments are orthogonal to the a-b plane in RuO₂ [15], while in MnTe, FeSb₂, Nb₂FeB₂ and Ta₂FeB₂ the moments are predicted to be in-plane [27, 32, 38]. By examining analytic expressions for the Landau coefficients derived from realistic microscopic models, we elucidate how the structure of SOC allows for the AM anisotropy energy to be understood.

Interplay between magnetization and AM Néel order.— Introducing \vec{N} as the intra-unit cell Néel order and \vec{M} as the magnetization, the general form of the free energy density in the presence of SOC can be written as

$$F = \frac{a_N}{2} \vec{N}^2 + \frac{b_N}{4} \vec{N}^4 + \frac{a_M}{2} \vec{M}^2 - \vec{h} \cdot \vec{M} + c_{ij} M_i N_j + s_1 (N_x^2 - N_y^2) + s_2 (N_x^2 + N_y^2 - 2N_z^2), \quad (1)$$

where a_N , b_N , a_M and c_{ij} are temperature-dependent Landau coefficients, \vec{h} is an applied field, and s_1 and s_2 are the coefficients determining the magnetic anisotropy energy due to SOC. Note that the bilinear coupling between the two orders M_i and N_j is only allowed in the

TABLE I. Lowest order free energy invariant between M_i and N_j in the presence of SOC for different point groups P and IRs of the spin splitting Γ_N , with the function $f_{\Gamma_N}(\mathbf{k})$ transforming as Γ_N . The last column indicates if the M_i generated from the AM order parameter is linear order in the SOC, denoted by a check mark, or higher order in SOC, denoted by a cross.

P	Γ_N	$f_{\Gamma_N}(\mathbf{k})$	Lowest order invariant	M_i linear in SOC
C_{2h}	B_g	$\alpha k_x k_z + \beta k_y k_z$	$\alpha_1 N_x M_z, \alpha_2 N_y M_z$ $\alpha_3 N_z M_y, \alpha_4 N_z M_x$	✓
D_{2h}	B_{1g}	$k_x k_y$	$\alpha_1 M_x N_y + \alpha_2 M_y N_x$	✓
D_{2h}	B_{2g}	$k_x k_z$	$\alpha_1 M_y N_z + \alpha_2 M_z N_y$	✓
D_{2h}	B_{3g}	$k_y k_z$	$\alpha_1 M_z N_x + \alpha_2 M_x N_z$	✓
C_{4h}	B_g	$\alpha(k_x^2 - k_y^2) + \beta k_x k_y$	$M_x N_y + M_y N_x, M_x N_x - M_y N_y$	✗
D_{4h}	A_{2g}	$k_x k_y (k_x^2 - k_y^2)$	$M_x N_y - M_y N_x$	✓
D_{4h}	B_{1g}	$k_x^2 - k_y^2$	$M_x N_x - M_y N_y$	✗
D_{4h}	B_{2g}	$k_x k_y$	$M_x N_y + M_y N_x$	✗
D_{3d}	A_{2g}	$k_x k_z (k_x^2 - 3k_y^2)$	$M_x N_y - M_y N_x$	✓
C_{6h}	B_g	$\alpha k_y k_z (k_y^2 - 3k_x^2) + \beta k_x k_z (k_x^2 - 3k_y^2)$	$\alpha M_z N_y (3N_x^2 - N_y^2) + \beta M_z N_x (3N_y^2 - N_x^2)$	✗
D_{6h}	A_{2g}	$k_x k_y (k_x^2 - 3k_y^2) \times (k_y^2 - 3k_x^2)$	$M_x N_y - M_y N_x$	✓
D_{6h}	B_{1g}	$k_y k_z (3k_x^2 - k_y^2)$	$M_z N_y (3N_x^2 - N_y^2)$	✗
D_{6h}	B_{2g}	$k_x k_z (k_x^2 - 3k_y^2)$	$M_z N_x (N_x^2 - 3N_y^2)$	✗
O_h	A_{2g}	$k_x^4 (k_x^2 - k_y^2) + k_y^4 (k_y^2 - k_x^2) + k_z^4 (k_x^2 - k_y^2)$	$M_x N_x (N_y^2 - N_z^2) + M_y N_y (N_z^2 - N_x^2) + M_z N_z (N_x^2 - N_y^2)$	✗

presence of SOC [23]. Without SOC, the spin-space group rotations, $[R_S || R_G]$, with spin space (R_S) and real space group operations (R_G) are uncoupled, which forces the bilinear coupling to vanish since \vec{N} is non-trivial under pure R_G operations. In the magnetic space group, the rotations act simultaneously on both spaces, and therefore R_S and the rotation portion of R_G must be the same, allowing this bilinear coupling to be non-zero. Eq. (1) describes orthorhombic or higher-symmetry point groups, for monoclinic groups see the supplementary material (SM) [39].

The lowest order invariant coupling M_i and N_j can be determined from symmetry analysis. The magnetization \vec{M} belongs to the axial vector irreducible representation (IR) Γ_A , see SM [39]. In contrast, \vec{N} belongs to the IR $\Gamma_A \otimes \Gamma_N$, with Γ_N the IR denoting the symmetry of the AM spin splitting. Hence, a coupling of M_i and N_j exists if the direct product $\Gamma_A \otimes \Gamma_A \otimes \Gamma_N$ contains the IR transforming trivially under all point group operations or, equivalently, there is a free energy invariant if $\Gamma_A \otimes \Gamma_A$ contains Γ_N [23]. In Table I we provide the form of the free energy invariants considering the relevant point groups and symmetries for the spin splitting identified in Ref. [35]. Note that for C_{6h} , O_h and certain IRs Γ_N of D_{6h} , a bilinear coupling is not allowed, and therefore the coupling is of higher order. Following a similar procedure, the lowest-order coupling between the magnetization and

the Néel vector can also be identified [39, 40], and is included in Table I.

Microscopic models.— To investigate the dependence of the induced FM spin moment on the SOC strength, we initially consider the general form of the minimal model for AM from Ref. [35], and carry out a model-independent quasi-symmetry based analysis later. Thus, we start from the normal state Hamiltonian

$$H_0 = \varepsilon_{0,\mathbf{k}} + t_{x,\mathbf{k}} \tau_x + t_{z,\mathbf{k}} \tau_z + \tau_y \vec{\lambda}_{\mathbf{k}} \cdot \vec{\sigma}, \quad (2)$$

where τ_i represent sublattice and σ_i spin degrees of freedom. The specific form of the parameters entering the model depends on the space group, the point group and the Wyckoff site symmetry. Here, $t_{x,\mathbf{k}}$ is an inter-sublattice hopping term, $\varepsilon_{0,\mathbf{k}}$ is the sublattice independent dispersion, and $\vec{\lambda}_{\mathbf{k}}$ is the SOC. The crystal asymmetric hopping term $t_{z,\mathbf{k}}$ exhibits a \mathbf{k} dependence that transforms as the non-trivial IR Γ_N since it describes the local symmetry breaking from multipole moments [35, 41, 42].

Initially, we analyze the AHE. For the Néel order along the an arbitrary direction l , N_l , the only contribution to the Berry curvature that is linear in SOC originates from the SOC component parallel to l , that is λ_l , and is given by [35, 39]

$$\begin{aligned} \Omega_{\alpha,\beta,ij}^{(N_l)} = & \frac{1}{2E_{\alpha,\beta}^3} \sum_{m,n=i,j} \varepsilon_{mn} \left[(N_l + \beta |t_{z,\mathbf{k}}|) \partial_m \lambda_{l,\mathbf{k}} \partial_n t_{x,\mathbf{k}} \right. \\ & + \text{sgn}(t_{z,\mathbf{k}}) \beta t_{x,\mathbf{k}} \partial_m t_{z,\mathbf{k}} \partial_n \lambda_{l,\mathbf{k}} \\ & \left. + \text{sgn}(t_{z,\mathbf{k}}) \beta \lambda_{l,\mathbf{k}} \partial_m t_{x,\mathbf{k}} \partial_n t_{z,\mathbf{k}} \right], \end{aligned} \quad (3)$$

where the dispersion is $E_{\alpha=\pm, \beta=\pm} = \alpha \left(N_l^2 + \lambda_{l,\mathbf{k}}^2 + t_{x,\mathbf{k}}^2 + t_{z,\mathbf{k}}^2 + 2\beta |N_l| |t_{z,\mathbf{k}}| \right)^{1/2}$. This expression is generically non-zero. Thus, when allowed by symmetry, the AHE is expected to be large and linear in SOC for all point groups and AM symmetries. In the SM [39], we carry out calculations of the AHE that support this conclusion.

To study now the interplay of the Néel order \vec{N} and the induced \vec{M} , we consider the perturbation

$$H' = \tau_z \vec{N} \cdot \vec{\sigma} + \vec{M} \cdot \vec{\sigma} \quad (4)$$

to the normal state Hamiltonian. We calculate the corrections to the normal state free energy close to the critical temperature as the magnetic order sets in by evaluating the loop expansion of the free energy. To second order it reads

$$F^{(2)} = \frac{1}{2\beta} \sum_{i\omega_n} \text{Tr}[G_0 H' G_0 H']. \quad (5)$$

Here, the bare Green's function projected to the band basis is given by

$$G_0(\mathbf{k}, i\omega_n) = \sum_{a=\pm} G_0^a(\mathbf{k}, i\omega_n) |u_{\mathbf{k}}^a\rangle \langle u_{\mathbf{k}}^a|, \quad (6)$$

where $G_0^{(\pm)}(\mathbf{k}, i\omega_n) = \frac{1}{i\omega_n - (\varepsilon_{0,\mathbf{k}} \pm \tilde{E}_{\mathbf{k}})}$ denotes the Green's function in the band basis, with the two-fold degenerate eigenenergies $E_{\mathbf{k}}^{\pm} = \varepsilon_{0,\mathbf{k}} \pm \tilde{E}_{\mathbf{k}}$ with $\tilde{E}_{\mathbf{k}} = \sqrt{t_{x,\mathbf{k}}^2 + t_{z,\mathbf{k}}^2 + \tilde{\lambda}_{\mathbf{k}}^2}$. The projection operator $P_{\mathbf{k}}^a = |u_{\mathbf{k}}^a\rangle \langle u_{\mathbf{k}}^a|$ in Eq. (6) transforms from the sublattice basis onto band a at wavevector \mathbf{k} [39, 43].

To examine the bilinear coupling between \vec{N} and \vec{M} , we derive an expression for the coefficient c_{ij} in Eq. (1). The analytic expressions for the other coefficients in Eq. (1) can be found in the SM [39]. At one-loop level, the quadratic free energy contribution in Eq. (5) coupling \vec{M} and \vec{N} is given by

$$F_{NM}^{(2)} = \frac{1}{\beta} \text{Tr} \left[\sum_{a,b,i\omega_n} G^a(\mathbf{k}, i\omega_n) G^b(\mathbf{k}, i\omega_n) \tau_z \vec{N} \cdot \vec{\sigma} P_{\mathbf{k}}^a \vec{M} \cdot \vec{\sigma} P_{\mathbf{k}}^b \right]. \quad (7)$$

Calculating the trace and performing the Matsubara frequency sum, we obtain

$$F_{NM}^{(2)} = 2 \sum_{\mathbf{k}} \frac{t_{x,\mathbf{k}}}{\tilde{E}_{\mathbf{k}}^2} L(\mathbf{k}) \vec{\lambda}_{\mathbf{k}} \cdot (\vec{M} \times \vec{N}), \quad (8)$$

with the function

$$L(\mathbf{k}) = \frac{df(\varepsilon)}{d\varepsilon} \Bigg|_{\varepsilon=E_{\mathbf{k}}^+} + \frac{df(\varepsilon)}{d\varepsilon} \Bigg|_{\varepsilon=E_{\mathbf{k}}^-} - \frac{2[f(E_{\mathbf{k}}^-) - f(E_{\mathbf{k}}^+)]}{E_{\mathbf{k}}^- - E_{\mathbf{k}}^+}, \quad (9)$$

incorporating the density of states and Lindhard term. The combination $(\vec{M} \times \vec{N})$ in Eq. (8) reveals that a nonzero invariant exists only if the antisymmetric direct product of the two axial IRs $[\Gamma_A \otimes \Gamma_A]_-$ contains Γ_N . In Table I we list whether the invariant can be generated to linear order of SOC, the antisymmetric product for the different point groups is detailed in the SM [39]. The SOC is expected to be a weak effect in AM [19], and therefore the induced magnetization will be vanishingly small when it is not generated to linear order. As seen from Table I, for the point group D_{4h} the SOC-linear invariant is only generated for $\Gamma_N = A_{2g}$. Focusing on crystals with rutile structure i.e. space group (SG) 136 and Wyckoff position 2a for the magnetic atoms as in RuO₂, MnF₂, NiF₂, and CoF₂, we have $\Gamma_N = B_{2g}$. Consequently, the induced \vec{M} is at least quadratic in SOC, as opposed to the material candidates Nb₂FeB₂ and Ta₂FeB₂, which have $\Gamma_N = A_{2g}$. Notably, Table I also shows that the FM moment induced in orthorhombic materials (D_{2h}) is generally expected to be larger.

To further verify these points, in Fig. 1 we show the calculated $\vec{M} = \mu_B \sum_{a,\mathbf{k}} \langle u_{\mathbf{k}}^a | \vec{S} | u_{\mathbf{k}}^a \rangle f(E_{\mathbf{k}}^a)$ relevant for (a) rutile structure (D_{4h} , $\Gamma_N = B_{2g}$) and (b) FeSb₂ structure (D_{2h} , $\Gamma_N = B_{1g}$). As seen, the SOC-induced \vec{M} indeed scales quadratically (linearly) with the SOC strength for SG 136 (FeSb₂) and is significantly smaller for the band relevant for rutile AM compared to FeSb₂.

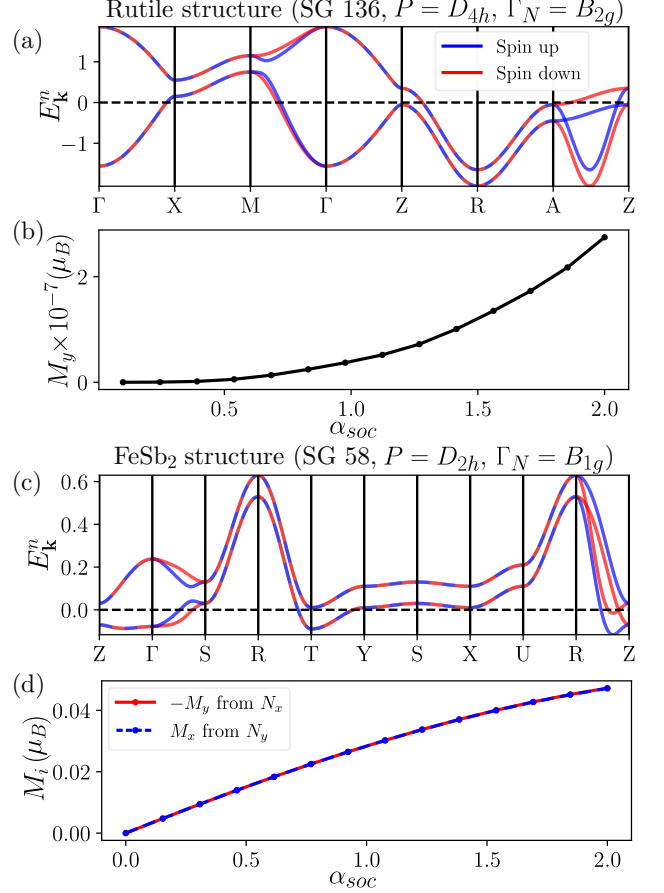


FIG. 1. Minimal model band structures and induced magnetization as a function of SOC strength for RuO₂ (a)-(b) vs FeSb₂ (c)-(d). We take $\vec{\lambda} = \alpha_{soc} \vec{\lambda}_0$, with $\vec{\lambda}_0 = (0.05, 0.05, 0.17)$ eV and $N_x = 0.2$ for RuO₂, and $\vec{\lambda}_0 = (2.7, 6.6, 75)$ meV and $N_x = 0.05$ for FeSb₂, both estimated from DFT results (see SM [39]). In agreement with Table I, \vec{M} is induced along the y axis for N_x , and scales quadratically (linearly) with the SOC strength for RuO₂ (FeSb₂). In (d) we show also the case with the Néel vector along the y -axis N_y , inducing $M_x \simeq -M_y$.

For the case of FeSb₂ we additionally compare the induced \vec{M} for the Néel vector along the x -axis and the y -axis in Fig. 1(d) to see if \vec{M} follows the predicted microscopic ($M_x N_y - M_y N_x$) result for the invariant. Indeed, even though M_x and M_y are not symmetry-related in this orthorhombic system, they are of opposite sign and nearly identical in magnitude for this material. In summary, these results explicitly demonstrate the properties summarized in Table I, which can be applied to gain similar insight for many classes of AM materials.

Finally, we note that in order to understand the quadratic dependence of \vec{M} on SOC from exact diagonalization, when \vec{M} is not allowed to linear order, requires the inclusion of secondary order parameters [23], equivalent to two-loop calculations [39]. Specifically, when

AM order sets in, secondary order parameters are also induced by symmetry, and they can give rise to a finite coupling between the two orders \vec{M} and \vec{N} . Such secondary order parameters include other spin textures as well as a current loop order, see SM [39]. The free energy for a secondary order parameter \vec{O} can be written as

$$F = \gamma^{(1)} \vec{O}^2 + \gamma_{ij}^{(2)} N_i O_j + \gamma_{ij}^{(3)} M_i O_j, \quad (10)$$

which couples bilinearly to \vec{M} and \vec{N} . Thus, \vec{N} can also induce a magnetization \vec{M} through the secondary order parameter \vec{O} , and our minimal models reveal that in this case the FM spin moment is at least quadratic in SOC, as discussed in the SM [39].

Quasi-symmetry protection of negligible FM.— Our minimal models are in agreement with the DFT results, which suggests a more general explanation beyond specific loop expansions or microscopic models. Indeed, it is possible to understand the above results using the recently introduced concept of quasi-symmetry [36, 37], describing emergent approximate symmetries when certain terms in the Hamiltonian become negligible. Here we use SOC to generate our quasi-symmetry. Specifically, we consider the quasi-symmetry that emerges when two of the SOC components (λ_x , λ_y , or λ_z) vanish, as illustrated in Fig. 2 for a tetragonal system. The resulting symmetry group, which we denote the uniaxial spin-space group due to its spin rotational invariance around the SOC direction, has higher symmetry than the magnetic space group but lower symmetry than the spin space group. This is relevant for determining which Landau coefficients are linear in one of $\lambda_{x,y,z}$. For example, for $\lambda_z \neq 0$ with $\lambda_x = \lambda_y = 0$, the normal state Hamiltonian gains additional symmetries, i.e., quasi-symmetries. Importantly, whether the λ_z -linear contribution to the Landau coefficient is permitted depends not only on the intrinsic symmetries of the crystal, but also on these emergent quasi-symmetries [36, 37].

Here, we apply this to the Landau coefficients of $M_x N_y$ and $M_y N_x$. When only λ_x (λ_y) SOC is present, the normal state Hamiltonian acquires an additional two-fold spin-rotational symmetry $[C_{2x}||E]$ ($[C_{2y}||E]$), see Fig. 2(a) (Fig. 2(b)), which prohibits λ_x (or λ_y)-linear contribution to these two Landau coefficients since M_x (N_x) is odd under this quasi-symmetry while N_y (M_y) is even. When only λ_z is present, a relevant quasi-symmetry in the uniaxial spin point group is the four-fold spin-rotational symmetry $[C_{4z}||E]$. As seen from Fig. 2(c), under this symmetry the SOC-linear contribution to $M_x N_y$ and $M_y N_x$ coefficients must have opposite sign. This behavior is universal and applies to any space group, regardless of whether it has intrinsic 4-fold rotational symmetry, as demonstrated in Fig. 1(d) for FeSb₂. In structures with SG 136, however, its intrinsic tetragonal crystal symmetries force these two coefficients to be identical at all orders of SOC. Consequently, the SOC

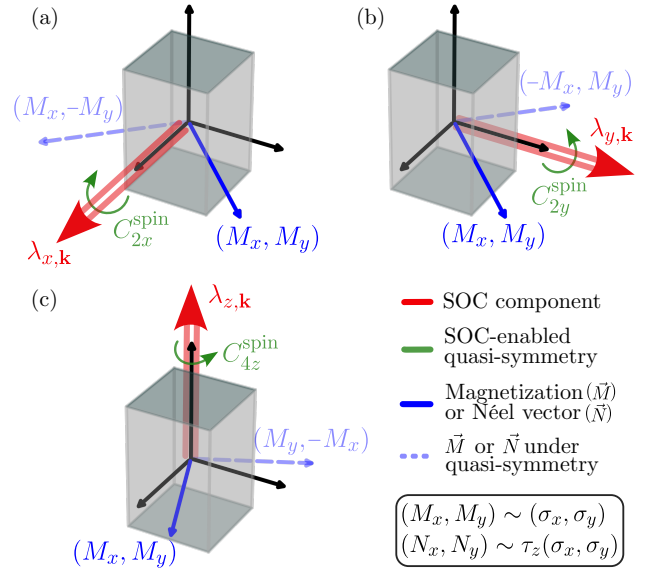


FIG. 2. SOC-enabled quasi-symmetry in a tetragonal system when only a single SOC component (a) $\lambda_{x,\mathbf{k}}$, (b) $\lambda_{y,\mathbf{k}}$ or (c) $\lambda_{z,\mathbf{k}}$ is present. The quasi-symmetry acts only in spin space, transforming the magnetization \vec{M} and the spin components of the Néel vector \vec{N} in the same way.

linear contribution must vanish, as shown in Fig. 1(b). The complete discussion on other space groups can be found in SM [39]. This also implies that for MnTe and CrSb, which have point group D_{6h} and $\Gamma_N = B_{1g}$, the FM moment will be cubic in SOC (see End Matter), independent of the non-linear coupling terms in Table I, in agreement with Refs. [27, 31]. Hence, the SOC enabled quasi-symmetry demonstrates that the results of the microscopic model are very general, and naturally explains when the FM spin moment is large or small depending on the AM symmetry. The only assumption on the microscopic Hamiltonian that underlies this analysis is that AM is an instability purely in the spin-channel, that is, it is driven only by exchange interactions without any orbital angular momentum contribution.

The relationship between the SOC direction and non-vanishing AHE in Eq. (3) can also be understood using SOC-based quasi-symmetry arguments like those given above, which do not depend on the form of the microscopic model. Specifically, the AHE measures current and voltage response, and hence is even under spin-rotational symmetries. For the Néel order along \hat{x} , when only the λ_y (λ_z) SOC is kept, the Néel order is odd under the resulting quasi-spin-rotational symmetry $[C_{2y}||E]$ ($[C_{2z}||E]$). This prevents a λ_y (λ_z)-linear SOC contribution to the AHE. When only the λ_x SOC is kept, the Néel order is even under the resulting $[C_{2x}||E]$ symmetry, and therefore the λ_x -linear contribution to AHE is allowed by the quasi-symmetry. It naturally follows that the AHE is given by the SOC component that is parallel to the Néel

vector.

Magnetic anisotropy energy.— The presence of SOC leads to a preferred direction for the Néel vector. As seen from the free energy in Eq. (1), this is captured by the s_1 and s_2 Landau coefficients. Thus, deriving analytic expressions for these coefficients from the microscopic models is useful to provide insight into the easy axis direction. Using the general microscopic model in Eq. (2) and focusing on the quadratic free energy correction due to SOC (see Eq. (5)), the coefficients can be written as

$$s_1 = -\frac{1}{2} \sum_{\mathbf{k}} \frac{\lambda_{x,\mathbf{k}}^2 - \lambda_{y,\mathbf{k}}^2}{\tilde{E}_{\mathbf{k}}^2} L(\mathbf{k}), \quad (11)$$

$$s_2 = -\frac{1}{6} \sum_{\mathbf{k}} \frac{\lambda_{x,\mathbf{k}}^2 + \lambda_{y,\mathbf{k}}^2 - 2\lambda_{z,\mathbf{k}}^2}{\tilde{E}_{\mathbf{k}}^2} L(\mathbf{k}), \quad (12)$$

with the function $L(\mathbf{k})$ defined in Eq. (9). The sign of these coefficients fixes the easy axis for a specific AM material. For instance, focusing on SG 136, $\lambda_{z,\mathbf{k}}$ can be ignored as it is smaller than $\lambda_{x,\mathbf{k}}$ and $\lambda_{y,\mathbf{k}}$ [35]. Hence, in general we expect that $s_2 > 0$ and, as a consequence, the easy axis is out of plane. However, Eqs. (11)-(12) also reveal that the moment direction may switch depending on the Fermi energy. In particular, when the Lindhard function (interband term in $L(\mathbf{k})$) dominates over the density of states (intraband term), $L(\mathbf{k})$ can change sign leading to $s_2 < 0$ and in-plane moment orientation. The switch of the AM moments as a function of the Fermi energy from the c -axis to the in-plane direction has been reported in Ref. [15] for RuO_2 . As shown in the SM, calculations of s_1 and s_2 for a minimal model of RuO_2 indeed yield $s_1 = 0$, $s_2 > 0$. In addition, application to FeSb_2 reveal that $s_1 > 0$, $s_2 < 0$, i.e. moments aligned along the in-plane y -axis, in agreement with DFT studies [32]. A systematic application of the magnetic anisotropy energy based on Eqs. (11)-(12) to other AM is beyond the scope of this work, and constitute an interesting future project.

Conclusions.— In summary, we have applied recently-developed realistic microscopic models for AM to derive relevant Landau coefficients of the free energy, focusing on the coupling between magnetization and Néel order, and magnetic anisotropy energies. The results explain the generic large AHE and the observed strong material-dependence of the SOC-induced weak FM. We stress that the weak FM described in this work refers to the spin moment. For materials where this moment is forbidden to linear order, e.g. the rutiles, secondary orders become relevant, and the orbital magnetic moment may also yield contributions to the small but finite net magnetization [18, 44]. Finally, we discovered a general quasi-symmetry enabled by the SOC that is model-independent and allows to determine for which AM symmetries the induced FM spin moment is large or vanishingly small.

Acknowledgements.— M. R. acknowledges support from the Novo Nordisk Foundation grant NNF20OC0060019.

A. K. acknowledges support by the Danish National Committee for Research Infrastructure (NUFI) through the ESS-Lighthouse Q-MAT. D. F. A. and Y. Y. were supported by the National Science Foundation Grant No. DMREF 2323857. Work at UWM was also supported by a grant from the Simons Foundation (SFI-MPS-NFS-00006741-02, D.F.A and M.R.).

- [1] Naoto Nagaosa, Jairo Sinova, Shigeki Onoda, A. H. MacDonald, and N. P. Ong, “Anomalous Hall effect,” *Rev. Mod. Phys.* **82**, 1539–1592 (2010).
- [2] Inti Sodemann and Liang Fu, “Quantum Nonlinear Hall Effect Induced by Berry Curvature Dipole in Time-Reversal Invariant Materials,” *Phys. Rev. Lett.* **115**, 216806 (2015).
- [3] Anyuan Gao, Yu-Fei Liu, Jian-Xiang Qiu, Barun Ghosh, Thaís V. Trevisan, Yugo Onishi, Chaowei Hu, Tiema Qian, Hung-Ju Tien, Shao-Wen Chen, Mengqi Huang, Damien Bérubé, Houchen Li, Christian Tzschaschel, Thao Dinh, *et al.*, “Quantum metric nonlinear Hall effect in a topological antiferromagnetic heterostructure,” *Science* **381**, 181–186 (2023).
- [4] Daniel Kaplan, Tobias Holder, and Binghai Yan, “Unification of Nonlinear Anomalous Hall Effect and Nonreciprocal Magnetoresistance in Metals by the Quantum Geometry,” *Phys. Rev. Lett.* **132**, 026301 (2024).
- [5] Yuan Fang, Jennifer Cano, and Sayed Ali Akbar Ghosh, “Quantum Geometry Induced Nonlinear Transport in Altermagnets,” *Phys. Rev. Lett.* **133**, 106701 (2024).
- [6] Z. Z. Du, Hai-Zhou Lu, and X. C. Xie, “Nonlinear Hall effects,” *Nature Reviews Physics* **3**, 744–752 (2021).
- [7] Naizhou Wang, Daniel Kaplan, Zhaowei Zhang, Tobias Holder, Ning Cao, Aifeng Wang, Xiaoyuan Zhou, Feifei Zhou, Zhengzhi Jiang, Chusheng Zhang, Shihao Ru, Hongbing Cai, Kenji Watanabe, Takashi Taniguchi, Binghai Yan, and Weibo Gao, “Quantum-metric-induced nonlinear transport in a topological antiferromagnet,” *Nature* **621**, 487–492 (2023).
- [8] Suyoung Lee, Sangjae Lee, Saegyeol Jung, Jiwon Jung, Donghan Kim, Yeonjae Lee, Byeongjun Seok, Jaeyoung Kim, Byeong Gyu Park, Libor Šmejkal, Chang-Jong Kang, and Changyoung Kim, “Broken Kramers Degeneracy in Altermagnetic MnTe,” *Phys. Rev. Lett.* **132**, 036702 (2024).
- [9] J. Krempaský, L. Šmejkal, S. W. D’Souza, M. Hajaoui, G. Springholz, K. Uhlířová, F. Alarab, P. C. Constantinou, V. Strocov, D. Usanov, W. R. Pudelko, R. González-Hernández, A. Birk Hellenes, Z. Jansa, H. Reichlová, Z. Šobáň, R. D. Gonzalez Betancourt, P. Wadley, J. Sinova, D. Kriegner, J. Minár, J. H. Dil, and T. Jungwirth, “Altermagnetic lifting of Kramers spin degeneracy,” *Nature* **626**, 517–522 (2024).
- [10] T. Osumi, S. Souma, T. Aoyama, K. Yamauchi, A. Honma, K. Nakayama, T. Takahashi, K. Ohgushi, and T. Sato, “Observation of a giant band splitting in altermagnetic MnTe,” *Phys. Rev. B* **109**, 115102 (2024).
- [11] Cong Li, Mengli Hu, Zhilin Li, Yang Wang, Wanyu Chen, Balasubramanian Thiagarajan, Mats Leandersson, Craig Polley, Timur Kim, Hui Liu, Cosma Fulga, Maia G.

Vergniory, Oleg Janson, Oscar Tjernberg, and Jeroen van den Brink, “Topological Weyl Altermagnetism in CrSb,” *arXiv* (2024), [10.48550/arXiv.2405.14777](https://arxiv.org/abs/2405.14777), [2405.14777](https://arxiv.org/abs/2405.14777).

[12] Guowei Yang, Zhanghuan Li, Sai Yang, Jiyuan Li, Hao Zheng, Weifan Zhu, Ze Pan, Yifu Xu, Saizheng Cao, Wenxuan Zhao, Anupam Jana, Jiawen Zhang, Mao Ye, Yu Song, Lun-Hui Hu, Lexian Yang, Jun Fujii, Ivana Vobornik, Ming Shi, Huiqiu Yuan, Yongjun Zhang, Yuanfeng Xu, and Yang Liu, “Three-dimensional mapping of the altermagnetic spin splitting in CrSb,” *Nature Communications* **16**, 1442 (2025).

[13] Sonka Reimers, Lukas Odenbreit, Libor Šmejkal, Vladimir N. Strocov, Prokopios Constantinou, Anna B. Hellenes, Rodrigo Jaeschke Ubiergo, Warlley H. Campos, Venkata K. Bharadwaj, Atasi Chakraborty, Thibaud Denneulin, Wen Shi, Rafal E. Dunin-Borkowski, Suvadip Das, Mathias Kläui, Jairo Sinova, and Martin Jourdan, “Direct observation of altermagnetic band splitting in CrSb thin films,” *Nat. Commun.* **15**, 1–7 (2024).

[14] Jianyang Ding, Zhicheng Jiang, Xiuhua Chen, Zicheng Tao, Zhengtai Liu, Tongrui Li, Jishan Liu, Jianping Sun, Jinguang Cheng, Jiayu Liu, Yichen Yang, Runfeng Zhang, Liwei Deng, Wenchuan Jing, Yu Huang, Yuming Shi, Mao Ye, Shan Qiao, Yilin Wang, Yanfeng Guo, Donglai Feng, and Dawei Shen, “Large Band Splitting in *g*-Wave Altermagnet CrSb,” *Phys. Rev. Lett.* **133**, 206401 (2024).

[15] Zexin Feng, Xiaorong Zhou, Libor Šmejkal, Lei Wu, Zengwei Zhu, Huixin Guo, Rafael González-Hernández, Xiaoning Wang, Han Yan, Peixin Qin, Xin Zhang, Hao-jiang Wu, Hongyu Chen, Ziang Meng, Li Liu, Zhengcai Xia, Jairo Sinova, Tomáš Jungwirth, and Zhiqi Liu, “An anomalous Hall effect in altermagnetic ruthenium dioxide,” *Nat. Electron.* **5**, 735–743 (2022).

[16] K. P. Kluczyk, K. Gas, M. J. Grzybowski, P. Skupiński, M. A. Borysiewicz, T. Fas, J. Suffczyński, J. Z. Domagala, K. Grasza, A. Mycielski, M. Baj, K. H. Ahn, K. Výborný, M. Sawicki, and M. Gryglas-Borysiewicz, “Coexistence of anomalous Hall effect and weak magnetization in a nominally collinear antiferromagnet MnTe,” *Phys. Rev. B* **110**, 155201 (2024).

[17] R. D. Gonzalez Betancourt, J. Zubáč, R. Gonzalez-Hernandez, K. Geishendorf, Z. Šobáň, G. Springholz, K. Olejník, L. Šmejkal, J. Sinova, T. Jungwirth, S. T. B. Goennenwein, A. Thomas, H. Reichlová, J. Železný, and D. Kriegner, “Spontaneous Anomalous Hall Effect Arising from an Unconventional Compensated Magnetic Phase in a Semiconductor,” *Phys. Rev. Lett.* **130**, 036702 (2023).

[18] Libor Šmejkal, Rafael González-Hernández, T. Jungwirth, and J. Sinova, “Crystal time-reversal symmetry breaking and spontaneous Hall effect in collinear antiferromagnets,” *Sci. Adv.* **6** (2020), [10.1126/sciadv.aaz8809](https://doi.org/10.1126/sciadv.aaz8809).

[19] Libor Šmejkal, Jairo Sinova, and Tomas Jungwirth, “Beyond Conventional Ferromagnetism and Antiferromagnetism: A Phase with Nonrelativistic Spin and Crystal Rotation Symmetry,” *Phys. Rev. X* **12**, 031042 (2022).

[20] Libor Šmejkal, Jairo Sinova, and Tomas Jungwirth, “Emerging Research Landscape of Altermagnetism,” *Phys. Rev. X* **12**, 040501 (2022).

[21] Libor Šmejkal, Allan H. MacDonald, Jairo Sinova, Satoru Nakatsuji, and Tomas Jungwirth, “Anomalous Hall antiferromagnets,” *Nat. Rev. Mater.* **7**, 482–496 (2022).

[22] Hai-Yang Ma, Mengli Hu, Nana Li, Jianpeng Liu, Wang Yao, Jin-Feng Jia, and Junwei Liu, “Multifunctional antiferromagnetic materials with giant piezomagnetism and noncollinear spin current,” *Nat. Commun.* **12**, 1–8 (2021).

[23] Paul A. McClarty and Jeffrey G. Rau, “Landau Theory of Altermagnetism,” *Phys. Rev. Lett.* **132**, 176702 (2024).

[24] Rui-Chun Xiao, Hui Li, Hui Han, Wei Gan, Mengmeng Yang, Ding-Fu Shao, Shu-Hui Zhang, Yang Gao, Mingliang Tian, and Jianhui Zhou, “Anomalous-Hall Neel textures in altermagnetic materials,” *arXiv* (2024), [10.48550/arXiv.2411.10147](https://arxiv.org/abs/2411.10147), [2411.10147](https://arxiv.org/abs/2411.10147).

[25] Rafael M. Fernandes, Vanuildo S. de Carvalho, Turan Birol, and Rodrigo G. Pereira, “Topological transition from nodal to nodeless Zeeman splitting in altermagnets,” *Phys. Rev. B* **109**, 024404 (2024).

[26] Sang-Wook Cheong and Fei-Ting Huang, “Altermagnetism with non-collinear spins,” *npj Quantum Mater.* **9**, 1–6 (2024).

[27] I. I. Mazin and K. D. Belashchenko, “Origin of the gosamer ferromagnetism in MnTe,” *Phys. Rev. B* **110**, 214436 (2024).

[28] T. Berlijn, P. C. Snijders, O. Delaire, H.-D. Zhou, T. A. Maier, H.-B. Cao, S.-X. Chi, M. Matsuda, Y. Wang, M. R. Koehler, P. R. C. Kent, and H. H. Weitering, “Itinerant Antiferromagnetism in RuO₂,” *Phys. Rev. Lett.* **118**, 077201 (2017).

[29] M. Hiraishi, H. Okabe, A. Koda, R. Kadono, T. Muroi, D. Hirai, and Z. Hiroi, “Nonmagnetic Ground State in RuO₂ Revealed by Muon Spin Rotation,” *Phys. Rev. Lett.* **132**, 166702 (2024).

[30] Philipp Kefler, Laura Garcia-Gassull, Andreas Suter, Thomas Prokscha, Zaher Salman, Dmitry Khalyavin, Pascal Manuel, Fabio Orlandi, Igor I. Mazin, Roser Valentí, and Simon Moser, “Absence of magnetic order in RuO₂: insights from μ SR spectroscopy and neutron diffraction,” *npj Spintronics* **2** (2024), [10.1038/s44306-024-00055-y](https://doi.org/10.1038/s44306-024-00055-y).

[31] Carmine Autieri, Raghottam M. Sattigeri, Giuseppe Cuono, and Amar Fakhredine, “Staggered Dzyaloshinskii-Moriya interaction inducing weak ferromagnetism in centrosymmetric altermagnets and weak ferrimagnetism in noncentrosymmetric altermagnets,” *Phys. Rev. B* **111**, 054442 (2025).

[32] Igor I. Mazin, Klaus Koepernik, Michelle D. Johannes, Rafael González-Hernández, and Libor Šmejkal, “Prediction of unconventional magnetism in doped FeSb₂,” *Proc. Natl. Acad. Sci. U.S.A.* **118**, e2108924118 (2021).

[33] Lotan Attias, Alex Levchenko, and Maxim Khodas, “Intrinsic anomalous hall effect in altermagnets,” *Phys. Rev. B* **110**, 094425 (2024).

[34] Marko Milivojević, Marko Orozović, Silvia Picozzi, Martin Gmitra, and Srđan Stavrić, “Interplay of altermagnetism and weak ferromagnetism in two-dimensional RuF₄,” *2D Mater.* **11**, 035025 (2024).

[35] Mercè Roig, Andreas Kreisel, Yue Yu, Brian M. Andersen, and Daniel F. Agterberg, “Minimal models for altermagnetism,” *Phys. Rev. B* **110**, 144412 (2024).

[36] Jiayu Li, Ao Zhang, Yuntian Liu, and Qihang Liu, “Group Theory on Quasisymmetry and Protected Near Degeneracy,” *Phys. Rev. Lett.* **133**, 026402 (2024).

[37] Chunyu Guo, Lunhui Hu, Carsten Putzke, Jonas Diaz, Xiangwei Huang, Kaustuv Manna, Feng-Ren Fan, Chandra Shekhar, Yan Sun, Claudia Felser, Chaoxing Liu, B. Andrei Bernevig, and Philip J. W. Moll, “Quasi-

symmetry-protected topology in a semi-metal,” *Nature Physics* **18**, 813–818 (2022).

[38] Xiao-Yao Hou, Huan-Cheng Yang, Zheng-Xin Liu, Peng-Jie Guo, and Zhong-Yi Lu, “Large intrinsic anomalous Hall effect in both Nb_2FeB_2 and Ta_2FeB_2 with collinear antiferromagnetism,” *Phys. Rev. B* **107**, L161109 (2023).

[39] Mercè Roig, Yue Yu, Rune C. Ekman, Andreas Kreisel, Brian M. Andersen, and Daniel F. Agterberg, “Supplementary Material for: Quasi-symmetry Constrained Spin Ferromagnetism in Altermagnets,”

[40] Matthias Hecker, Anant Rastogi, Daniel F. Agterberg, and Rafael M. Fernandes, “Classification of electronic nematicity in three-dimensional crystals and quasicrystals,” *Phys. Rev. B* **109**, 235148 (2024).

[41] Satoru Hayami, Megumi Yatsushiro, Yuki Yanagi, and Kusunose Hiroaki, “Classification of atomic-scale multi-

End Matter

Appendix: General SOC-enabled quasi-symmetry— As introduced in the main text, the quasi-symmetry generated by SOC when two of the SOC components vanish allows us to determine which Landau coefficients are linear in one of $\lambda_{x,y,z}$. As illustrated in Fig. 3, the resulting symmetry group, denoted here as the uniaxial spin space group, has lower symmetry than the spin space group, but higher symmetry than the magnetic space group. Here, we develop a more general quasi-symmetry criterion that addresses the following question: can a Landau coefficient or response function host a contribution from $\lambda_x^{n_x} \lambda_y^{n_y} \lambda_z^{n_z}$, for given integers $(n_x, n_y, n_z) \geq 0$?

We would like to consider a general Hamiltonian that can extend beyond the minimal models discussed in this paper. SOC terms can always be grouped into terms proportional to spin operators σ_x , σ_y , and σ_z . Terms in each group can carry different momentum and orbital dependence, with overall SOC strengths λ_x , λ_y , and λ_z :

$$H_{SOC} = \lambda_x(a_{1,\mathbf{k}}\hat{A}_1 + a_{2,\mathbf{k}}\hat{A}_2 + \dots)\sigma_x + \lambda_y(b_{1,\mathbf{k}}\hat{B}_1 + b_{2,\mathbf{k}}\hat{B}_2 + \dots)\sigma_y + \lambda_z(c_{1,\mathbf{k}}\hat{C}_1 + c_{2,\mathbf{k}}\hat{C}_2 + \dots)\sigma_z, \quad (13)$$

with momentum-dependent coefficients $a_i, b_i, c_i = O(1)$ and $\hat{A}_i, \hat{B}_i, \hat{C}_i$ some operators acting on sublattice and/or orbital space. The quasi-symmetry argument is based on analyticity of the response functions. If the DOS is not concentrated at singular regions such as band crossings, response functions should be an analytical function of $\lambda_{x,y,z}$. Cross-terms like $\sqrt{\lambda_x \lambda_y}$ are not allowed. For the minimal model, this property is explicitly shown in the normal-state Green’s function Eq. (6), where the projection operator is a linear combination of the three SOC terms.

We now interpret the three groups of SOC terms as

poles under crystallographic point groups and application to linear response tensors,” *Phys. Rev. B* **98**, 165110 (2018).

[42] Sayantika Bhowal and Nicola A. Spaldin, “Ferroically Ordered Magnetic Octupoles in d -Wave Altermagnets,” *Phys. Rev. X* **14**, 011019 (2024).

[43] Ansgar Graf and Frédéric Piéchon, “Berry curvature and quantum metric in N -band systems: An eigenprojector approach,” *Phys. Rev. B* **104**, 085114 (2021).

[44] Daegeun Jo, Dongwook Go, Yuriy Mokrousov, Peter M. Oppeneer, Sang-Wook Cheong, and Hyun-Woo Lee, “Weak Ferromagnetism in Altermagnets from Alternating g -Tensor Anisotropy,” *arXiv* (2024), 10.48550/arXiv.2410.17386, (accepted in PRL).

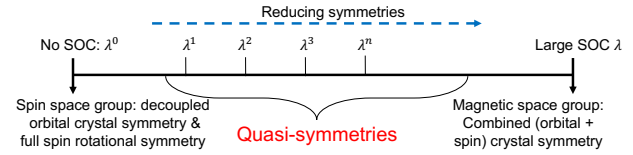


FIG. 3. Classification scheme of the spin space group and magnetic space group in terms of the strength and powers of SOC, illustrating when the quasi-symmetries emerge. In particular, when two of the SOC components vanish, the resulting symmetry group (which we denote as the uniaxial spin space group) has spin rotational invariance around the SOC direction.

distinct symmetry-breaking order parameters in a SOC-free system (spin-space group). The spin-space group hosts decoupled orbital crystal symmetries and full spin-rotational symmetries. General order parameters are denoted by $\vec{O}_{R,i}$, where R is the IR under orbital rotations and the index $i = 1, 2, \dots$ reflects its dimensionality. The vector notation indicates that each $\vec{O}_{R,i}$ also transforms as a spin vector under spin rotations.

Each group of SOC terms corresponds to a different symmetry breaking in this high-symmetry system. For example, consider the λ_z SOC term in a tetragonal system. It breaks spin-rotational symmetry as the spin vector σ_z , and it breaks orbital symmetry according to the 1D IR $A_{2g} \sim xy(x^2-y^2)$. It is then $\vec{O}_{A_{2g}} = (0, 0, \Lambda_z)$. For $\lambda_{x,y}$ SOC terms, they break spin-rotational symmetry as the spin vector $\sigma_{x,y}$, and they break orbital symmetry according to the 2D IR $E_g \sim \{xz, yz\}$. They are then $\vec{O}_{E_g,1} = (\Lambda_{xy}, 0, 0)$ and $\vec{O}_{E_g,2} = (0, \Lambda_{xy}, 0)$.

If the coefficient of a Landau term or response function X hosts a contribution from $\lambda_x^{n_x} \lambda_y^{n_y} \lambda_z^{n_z}$, then the term

$\Lambda_x^{n_x} \Lambda_y^{n_y} \Lambda_z^{n_z} X$ must be allowed in the Landau theory for the SOC-free system. We note that for the tetragonal system, the contributions from $\lambda_{x,y}^{n_{xy}} \lambda_z^{n_z}$ enable the term $\Lambda_{xy}^{n_{xy}} \Lambda_z^{n_z} X$ in the Landau theory for the SOC-free system (since $\lambda_x = \lambda_y$ in this case). In the SOC-free system, a valid Landau term should be a spin-scalar, and belong to the trivial IR under orbital rotations. This provides a general quasi-symmetry criterion.

Examples

1. In the SOC-free tetragonal D_{4h} systems, the SOC order parameters are: $\vec{O}_{E_g,1} = (\Lambda_{xy}, 0, 0)$, $\vec{O}_{E_g,2} = (0, \Lambda_{xy}, 0)$ and $\vec{O}_{A_{2g}} = (0, 0, \Lambda_z)$. Ferromagnetic order is $\vec{M}_{A_{1g}}$, and altermagnetic order is \vec{N}_P , with altermagnetic symmetry $\Gamma_N = P$. To have a SOC-linear coupling between an altermagnet and a ferromagnet, $\vec{O} \cdot (\vec{M} \times \vec{N})$ must be allowed. The altermagnetic symmetry thus has to be A_{2g} or E_g . For two atoms per nonmagnetic unit cell, only $\Gamma_N = A_{2g}, B_{1g}, B_{2g}$ are allowed [35].
 - (a) For $\Gamma_N = A_{2g}$, the Landau term $\vec{O}_{A_{2g}} \cdot (\vec{M}_{A_{1g}} \times \vec{N}_{A_{2g}}) = \Lambda_z(M_x N_y - M_y N_x)$ is allowed. Hence the λ_z -linear contribution to $M_x N_y - M_y N_x$ is nonzero.
 - (b) For $\Gamma_N = B_{2g}$ and Landau term $M_x N_y + M_y N_x$, SOC-linear terms are forbidden. Since $E_g \otimes E_g \otimes B_{2g}$ contains the trivial IR, the quadratic λ_{xy}^2 contribution is allowed. An example Landau term is $(\vec{O}_{E_g,1} \times \vec{M}) \cdot (\vec{N} \times \vec{O}_{E_g,2}) + (\vec{O}_{E_g,2} \times \vec{M}) \cdot (\vec{N} \times \vec{O}_{E_g,1}) = \Lambda_{xy}^2(M_x N_y + M_y N_x)$.
 - (c) For $\Gamma_N = B_{1g}$ and Landau term $M_x N_x - M_y N_y$, SOC-linear terms are forbidden. Since $E_g \otimes E_g \otimes B_{1g}$ contains the trivial IR, the quadratic λ_{xy}^2 contribution is allowed. An example Landau term is $(\vec{O}_{E_g,1} \times \vec{M}) \cdot (\vec{N} \times \vec{O}_{E_g,1}) - (\vec{O}_{E_g,2} \times \vec{M}) \cdot (\vec{N} \times \vec{O}_{E_g,2}) = \Lambda_{xy}^2(M_x N_x - M_y N_y)$.
2. In the SOC-free hexagonal D_{6h} systems, the SOC order parameters are: $\vec{O}_{E_{1g},1} = (\Lambda_{xy}, 0, 0)$, $\vec{O}_{E_{1g},2} = (0, \Lambda_{xy}, 0)$ and $\vec{O}_{A_{2g}} = (0, 0, \Lambda_z)$. To have a SOC-linear coupling between altermagnet and ferromagnet, $\vec{O} \cdot (\vec{M} \times \vec{N})$ must be allowed. Thus, $\Gamma_N = A_{2g}$ or E_{1g} . For two atoms per nonmagnetic unit cell, only A_{2g} , B_{1g} , and B_{2g} are allowed [35].
 - (a) The discussion for $\Gamma_N = A_{2g}$ is the same as A_{2g} in tetragonal systems.
 - (b) For $\Gamma_N = B_{1g}$ (similar for $\Gamma_N = B_{2g}$), MN^3 coupling has no SOC-linear contribution since $B_{1g} \otimes B_{1g} \otimes B_{1g} \otimes \{E_{1g}, A_{2g}\}$ has no trivial IR. Similarly, SOC-quadratic contribution is also forbidden since $B_{1g} \otimes B_{1g} \otimes \{E_{1g}, A_{2g}\} \otimes \{E_{1g}, A_{2g}\}$ has no trivial IR. $B_{1g} \otimes \{E_{1g}, A_{2g}\} \otimes \{E_{1g}, A_{2g}\}$ has no trivial IR. SOC-cubic contribution is allowed as $B_{1g} \otimes B_{1g} \otimes B_{1g} \otimes E_{1g} \otimes E_{1g} \otimes E_{1g}$ has trivial IR. The SOC dependence is cubic in λ_{xy} .

Supplementary Material for: "Quasi-symmetry Constrained Spin Ferromagnetism in Altermagnets"

Mercè Roig,¹ Yue Yu,² Rune C. Ekman,¹ Andreas Kreisel,¹ Brian M. Andersen,¹ and Daniel F. Agterberg²

¹*Niels Bohr Institute, University of Copenhagen, DK-2100 Copenhagen, Denmark*

²*Department of Physics, University of Wisconsin-Milwaukee, Milwaukee, Wisconsin 53201, USA*

In this supplementary material, we provide details on supporting derivations, resulting analytical expressions for all coefficients in the free energy, examples of secondary order parameters, general analytic expressions for the Berry curvature and a detailed analysis of the magnetic anisotropy energy.

S1. GENERAL FREE ENERGY IN THE PRESENCE OF SPIN-ORBIT COUPLING

In the main text we include the form of the free energy for orthorhombic and higher-symmetry groups. In the case of monoclinic groups, there are additional terms due to the lower crystal symmetry, and therefore the free energy can generally be written as

$$f = \frac{a_N}{2} \vec{N}^2 + \frac{b_N}{4} \vec{N}^4 + \frac{a_M}{2} \vec{M}^2 - \vec{h} \cdot \vec{M} + c_{ij} M_i N_j + s_1 (N_x^2 - N_y^2) + s_2 (N_x^2 + N_y^2 - 2N_z^2) + s_3 N_x N_y + s_4 N_x N_z + s_5 N_y N_z, \quad (\text{S1})$$

where the coefficients s_3 , s_4 and s_5 can also be calculated from the general microscopic model and are given by

$$s_3 = -2 \sum_{\mathbf{k}} \frac{\lambda_{x,\mathbf{k}} \lambda_{y,\mathbf{k}}}{\tilde{E}_{\mathbf{k}}^2} L(\mathbf{k}), \quad (\text{S2})$$

$$s_4 = -2 \sum_{\mathbf{k}} \frac{\lambda_{x,\mathbf{k}} \lambda_{z,\mathbf{k}}}{\tilde{E}_{\mathbf{k}}^2} L(\mathbf{k}), \quad (\text{S3})$$

$$s_5 = -2 \sum_{\mathbf{k}} \frac{\lambda_{y,\mathbf{k}} \lambda_{z,\mathbf{k}}}{\tilde{E}_{\mathbf{k}}^2} L(\mathbf{k}). \quad (\text{S4})$$

with the function $L(\mathbf{k}) = \frac{df(\varepsilon)}{d\varepsilon} \Big|_{\varepsilon=E_{\mathbf{k}}^+} + \frac{df(\varepsilon)}{d\varepsilon} \Big|_{\varepsilon=E_{\mathbf{k}}^-} - \frac{2[f(E_{\mathbf{k}}^-) - f(E_{\mathbf{k}}^+)]}{E_{\mathbf{k}}^- - E_{\mathbf{k}}^+}$. Here, $\tilde{E}_{\mathbf{k}} = \sqrt{t_{x,\mathbf{k}}^2 + t_{z,\mathbf{k}}^2 + \lambda_{\mathbf{k}}^2}$ are the eigenvalues of H_1 and the eigenvalues $E_{\mathbf{k}}^{\pm} = \varepsilon_{0,\mathbf{k}} \pm \tilde{E}_{\mathbf{k}}$ correspond to the full Hamiltonian in Eq. (2) of the main text. Note that the coefficients s_3 , s_4 and s_5 vanish for higher-symmetry groups.

S2. FREE ENERGY INVARIANTS COUPLING MAGNETIZATION AND NÉEL ORDER

As discussed in the main text, a bilinear coupling between the magnetization and the Néel order exists if the direct product $\Gamma_A \otimes \Gamma_A \otimes \Gamma_N$ contains the IR transforming trivially under all point group operations, where Γ_A is the axial vector irreducible representation (IR) and Γ_N is the IR denoting the symmetry of the spin splitting. Equivalently, there is a free energy invariant if $\Gamma_A \otimes \Gamma_A$ contains Γ_N . In Table S1 we detail the axial vector IR for the different point groups.

As an example, we consider the point group D_{4h} . In this case, $\Gamma_A = E_g \oplus A_{2g}$, and therefore $\Gamma_A \otimes \Gamma_A = 3A_{1g} \oplus 2E_g \oplus (E_g \otimes E_g)$. Neither A_{1g} or E_g belong to Γ_N (see Table I in the main text), so the invariants can only arise from $E_g \otimes E_g = A_{1g} \oplus A_{2g} \oplus B_{1g} \oplus B_{2g}$. Hence, for each of $\Gamma_N = A_{2g}, B_{1g}, B_{2g}$ there is an allowed bilinear coupling. To illustrate how to obtain the form of the invariant, we focus on the case $\Gamma_N = B_{2g}$. The magnetization \vec{M} belongs to the axial vector IR, and therefore transforms like the spin Pauli matrices, $(M_x, M_y, M_z) \sim (\sigma_x, \sigma_y, \sigma_z)$,

Table S1. Axial vector irreducible representation Γ_A and antisymmetric direct product $[\Gamma_A \otimes \Gamma_A]_-$ for all point groups considered in Table I of the main text.

P	C_{2h}	D_{2h}	C_{4h}	D_{4h}	D_{3d}	C_{6h}	D_{6h}	O_h
Γ_A	$B_g \oplus A_g$	$B_{1g} \oplus B_{2g} \oplus B_{3g}$	$A_g \oplus E_g$	$E_g \oplus A_{2g}$	$A_{2g} \oplus E_g$	$A_g \oplus E_{1g}$	$A_{2g} \oplus E_{1g}$	T_{1g}
$[\Gamma_A \otimes \Gamma_A]_-$	B_g	$B_{1g} \oplus B_{2g} \oplus B_{3g}$	A_g	A_{2g}	A_{2g}	A_g	A_{2g}	T_{1g}

while for the Néel order $(N_x, N_y, N_z) \sim \tau_z(\sigma_x, \sigma_y, \sigma_z)$ (see Eq. (3) in the main text). Since τ_z transforms like the crystal asymmetric hopping $t_{z,\mathbf{k}}$ it belongs to the IR Γ_N . Thus, in our particular example $\Gamma_N = B_{2g} \sim k_x k_y$ and $(\sigma_x, \sigma_y, \sigma_z) \sim (k_y k_z, k_x k_z, k_x k_y (k_x^2 - k_y^2))$. As a consequence, the only allowed invariant corresponds to $M_x N_y + M_y N_x$. Following this procedure, we have identified the invariants for the different point groups and symmetries of the altermagnetic spin splitting listed in Table I in the main text.

As seen from Table I in the main text, there are some cases where a bilinear coupling between \vec{M} and \vec{N} is not symmetry allowed. For instance, focusing on the point group D_{6h} , the axial IR corresponds to $\Gamma_A = A_{2g} \oplus E_{1g}$. Therefore, $\Gamma_A \otimes \Gamma_A = A_{1g} \oplus 2E_{1g} \oplus (E_{1g} \otimes E_{1g})$, with $E_{1g} \otimes E_{1g} = A_{1g} \oplus A_{2g} \oplus E_{2g}$, which implies that there is only a bilinear coupling for $\Gamma_N = A_{2g}$ and not for $\Gamma_N = B_{1g}, B_{2g}$. Similarly, a bilinear coupling is not allowed for C_{6h} and O_h . Consequently, to obtain the lowest-order invariant we have derived the coupling between \vec{M} and \vec{N} to third order. In these cases, an invariant is obtained if $(\Gamma_A \otimes \Gamma_A \otimes \Gamma_A)_{\text{sym}} \otimes \Gamma_A$ contains Γ_N , where sym denotes the symmetric product of three IRs [1]. The invariant is included in Table I of the main text.

S3. ANALYTIC EXPRESSION FOR THE COEFFICIENTS IN THE FREE ENERGY FROM MICROSCOPIC MODELS

In this section, we provide the analytic expressions for the coefficients a_N , b_N and a_M entering in the free energy in Eq. (1) of the main text using the microscopic model in Eq. (2) and the perturbation in Eq. (3). In the main text, we focus on the interplay between the magnetization and the Néel order, examining the expression for the c_{ij} coefficient, in addition to the coefficients s_1 and s_2 , which determine the magnetic anisotropy energy due to the effect of SOC.

We start by deriving an expression for the free energy density from the partition function Z as

$$\begin{aligned} F &= -\frac{1}{\beta} \log Z = -\frac{1}{\beta} \log \left[\int d\bar{c} d\bar{c} \exp(-cG^{-1}\bar{c}) \right] = -\frac{1}{\beta} \log \det(G^{-1}) = -\frac{1}{\beta} \sum_{i\omega_n} \text{Tr} \log(G^{-1}) \\ &= -\frac{1}{\beta} \sum_{i\omega_n} \text{Tr} \log(G_0^{-1} + H') = -\frac{1}{\beta} \sum_{i\omega_n} \text{Tr} [\log(G_0^{-1}) + \log(1 + G_0 H')] \\ &= -\frac{1}{\beta} \sum_{i\omega_n} \text{Tr} \log G_0^{-1} + \frac{1}{2\beta} \sum_{i\omega_n} \text{Tr}((G_0 H')^2) + \frac{1}{4\beta} \sum_{i\omega_n} \text{Tr}((G_0 H')^4), \end{aligned}$$

where G is the full Green's function, G_0 is the bare Green's function and H' is the perturbation to the normal-state Hamiltonian written in Eq. (3) of the main text, including the Néel order \vec{N} and the induced magnetization \vec{M} . In addition, $\beta = 1/k_B T$ and ω_n corresponds to the Matsubara frequency.

Hence, the second and fourth order corrections to the normal state free energy when the magnetic order sets in are evaluated from

$$F^{(2)} = \frac{1}{2\beta} \sum_{i\omega_n} \text{Tr}[G_0(\mathbf{k}, i\omega_n) H' G_0(\mathbf{k}, i\omega_n) H'], \quad (\text{S5})$$

$$F^{(4)} = \frac{1}{4\beta} \sum_{i\omega_n} \text{Tr}[(G_0(\mathbf{k}, i\omega_n) H')^4]. \quad (\text{S6})$$

The corresponding diagrammatic representation is illustrated in Fig. S1(a) and (b), respectively, where $\vec{\alpha}$ can denote both order parameters \vec{N} and \vec{M} . The bare Green's function projected to the band basis corresponds to

$$G_0(\mathbf{k}, i\omega_n) = \sum_{a=\pm} G_0^a(\mathbf{k}, i\omega_n) |u_{\mathbf{k}}^a\rangle \langle u_{\mathbf{k}}^a|, \quad (\text{S7})$$

where $G_0^{(\pm)}(\mathbf{k}, i\omega_n) = \frac{1}{i\omega_n - (\varepsilon_{0,\mathbf{k}} \pm \tilde{E}_{\mathbf{k}})}$ denotes the Green's function in the band basis, with the two-fold degenerate eigenenergies $E_{\mathbf{k}}^{\pm} = \varepsilon_{0,\mathbf{k}} \pm \tilde{E}_{\mathbf{k}}$ where $\tilde{E}_{\mathbf{k}} = \sqrt{t_{x,\mathbf{k}}^2 + t_{z,\mathbf{k}}^2 + \lambda_{\mathbf{k}}^2}$ are the eigenenergies of $H_1 = t_{x,\mathbf{k}} \tau_x + t_{z,\mathbf{k}} \tau_z + \tau_y \vec{\lambda}_{\mathbf{k}} \cdot \vec{\sigma}$. With this, we construct the projection operator [2, 3]

$$P_{\mathbf{k}}^a = |u_{\mathbf{k}}^a\rangle \langle u_{\mathbf{k}}^a| = \frac{1}{2} \left(\mathbb{1} + \frac{H_1}{\pm \tilde{E}_{\mathbf{k}}} \right) \quad (\text{S8})$$

from sublattice basis onto band a at wavevector \mathbf{k} .

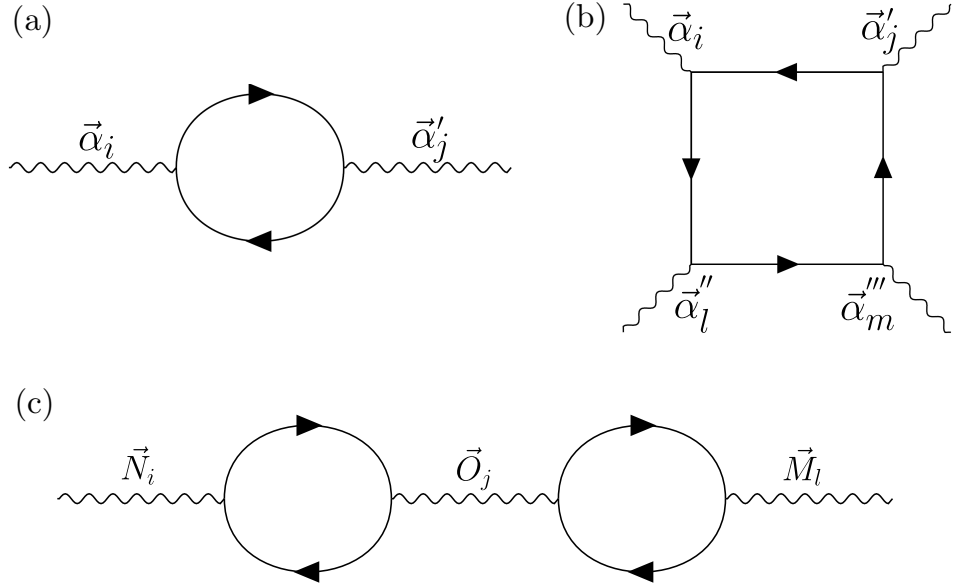


Figure S1. (a) Second-order and (b) fourth-order diagrams contributing to the free energy expansion where $\vec{\alpha}_i$, $\vec{\alpha}'_j$, $\vec{\alpha}''_l$ and $\vec{\alpha}'''_m$ can denote the components of the two magnetic orders \vec{M} and \vec{N} . (c) Two-loop diagram between \vec{N} and \vec{M} through a secondary order parameter \vec{O} .

We focus first on the term coupling the two Néel order parameters \vec{N} corresponding to the coefficient a_N in the free energy, obtaining

$$F_N^{(2)} = \frac{\vec{N}^2}{\beta} \sum_{\mathbf{k}, i\omega_n} \text{Tr} \left[\sum_{a,b} G^a(\mathbf{k}, i\omega_n) G^b(\mathbf{k}, i\omega_n) \tau_z |u_{\mathbf{k}}^a\rangle \langle u_{\mathbf{k}}^a| \tau_z |u_{\mathbf{k}}^b\rangle \langle u_{\mathbf{k}}^b| \right], \quad (\text{S9})$$

where we have replaced the Green's function projected in the band basis (see Eq. (S7)) into Eq. (S5). Note that the trace is over all degrees of freedom, including \mathbf{k} and the Matsubara frequency $i\omega_n$. Using the projector operator written in Eq. (S8), the expression for the free energy can be simplified to

$$F_N^{(2)} = \frac{\vec{N}^2}{\beta} \sum_{\mathbf{k}, i\omega_n} \frac{1}{t_{x,\mathbf{k}}^2 + t_{z,\mathbf{k}}^2} \left(2t_{x,\mathbf{k}}^2 G^-(\mathbf{k}, i\omega_n) G^+(\mathbf{k}, i\omega_n) + t_{z,\mathbf{k}}^2 [(G^-(\mathbf{k}, i\omega_n))^2 + (G^+(\mathbf{k}, i\omega_n))^2] \right). \quad (\text{S10})$$

Hence, performing the Matsubara frequency sum we identify

$$a_N = \frac{1}{U} + 2 \sum_{\mathbf{k}} \frac{1}{t_{x,\mathbf{k}}^2 + t_{z,\mathbf{k}}^2} \left\{ t_{x,\mathbf{k}}^2 \frac{2[f(E_{\mathbf{k}}^-) - f(E_{\mathbf{k}}^+)]}{E_{\mathbf{k}}^- - E_{\mathbf{k}}^+} + t_{z,\mathbf{k}}^2 \left[\frac{df(\varepsilon)}{d\varepsilon} \Big|_{\varepsilon=E_{\mathbf{k}}^+} + \frac{df(\varepsilon)}{d\varepsilon} \Big|_{\varepsilon=E_{\mathbf{k}}^-} \right] \right\}, \quad (\text{S11})$$

with $f(E_{\mathbf{k}}^a)$ denoting the Fermi function evaluated for the energy band a . Here, $\frac{1}{U}$ is the bare bosonic contribution from the Hubbard–Stratonovich transformation. This expression reveals that the susceptibility depends on the competition between the inter-band term and the intra-band term, as discussed in Ref. [3], and this determines whether ferromagnetism or Néel order is stabilized. Additionally, it also shows that band degeneracies help stabilizing altermagnetism.

We can follow the same procedure to obtain the a_M coefficient by focusing on the magnetization term in the perturbation. Thus, the free energy now simply reads

$$F_M^{(2)} = \frac{\vec{M}^2}{\beta} \sum_{\mathbf{k}, i\omega_n} [(G^-(\mathbf{k}, i\omega_n))^2 + (G^+(\mathbf{k}, i\omega_n))^2]. \quad (\text{S12})$$

Similarly to the previous case, the expression for the coefficient corresponds to

$$a_M = \frac{1}{U} + 2 \sum_{\mathbf{k}} \left\{ \frac{df(\varepsilon)}{d\varepsilon} \Big|_{\varepsilon=E_{\mathbf{k}}^+} + \frac{df(\varepsilon)}{d\varepsilon} \Big|_{\varepsilon=E_{\mathbf{k}}^-} \right\}. \quad (\text{S13})$$

In contrast to Eq. (S11), this coefficient contains only an intra-band term.

Finally, we can use Eq. (S6) to derive an expression for the quartic contribution to the free energy from the microscopic model, which corresponds to the diagram in Fig. S1(b). In this case, the expression for the coefficient b_N in the free energy expansion corresponds to

$$b_N = 4 \sum_{\mathbf{k}} \frac{1}{(t_{x,\mathbf{k}}^2 + t_{z,\mathbf{k}}^2)^2} \left\{ \frac{t_{x,\mathbf{k}}^4}{(E_{\mathbf{k}}^- - E_{\mathbf{k}}^+)^2} \left(f'(\varepsilon) \Big|_{\varepsilon=E_{\mathbf{k}}^+} + f'(\varepsilon) \Big|_{\varepsilon=E_{\mathbf{k}}^-} - 2 \frac{f(E_{\mathbf{k}}^-) - f(E_{\mathbf{k}}^+)}{E_{\mathbf{k}}^- - E_{\mathbf{k}}^+} \right) + \frac{t_{z,\mathbf{k}}^4}{12} \left(f'''(\varepsilon) \Big|_{\varepsilon=E_{\mathbf{k}}^+} + f'''(\varepsilon) \Big|_{\varepsilon=E_{\mathbf{k}}^-} \right) \right. \\ \left. + \frac{t_{x,\mathbf{k}}^2 t_{z,\mathbf{k}}^2}{E_{\mathbf{k}}^- - E_{\mathbf{k}}^+} \left(f''(\varepsilon) \Big|_{\varepsilon=E_{\mathbf{k}}^+} + f''(\varepsilon) \Big|_{\varepsilon=E_{\mathbf{k}}^-} - \frac{4}{E_{\mathbf{k}}^- - E_{\mathbf{k}}^+} \left[f'(\varepsilon) \Big|_{\varepsilon=E_{\mathbf{k}}^+} + f'(\varepsilon) \Big|_{\varepsilon=E_{\mathbf{k}}^-} \right] + 8 \frac{f(E_{\mathbf{k}}^-) - f(E_{\mathbf{k}}^+)}{(E_{\mathbf{k}}^- - E_{\mathbf{k}}^+)^2} \right) \right\}. \quad (\text{S14})$$

4. SECONDARY ORDER PARAMETERS

When a primary order parameter sets in, secondary order parameters are also induced by symmetry. As seen from Eq. (9) of the main text, these can induce a finite coupling between the Néel order \vec{N} and the magnetization \vec{M} . This process is equivalent to a 2-loop diagram between \vec{N} and \vec{M} , shown in Fig. S1(c). It should be noted that, the quasi-symmetry criteria is not limited to 1 or 2-loop diagrams. It is rather general and applies to all diagrams.

In this section, we focus on the tetragonal example with point group $P = D_{4h}$ and a symmetry for the spin splitting belonging to $\Gamma_N = B_{2g} \sim k_x k_y$, which is relevant for the rutile lattice (SG 136), and detail the form of the allowed secondary order parameters. Since in this case M_y and N_x transform like σ_y , $N_x \sim \tau_z \sigma_x$ can induce M_y through 11 different secondary order parameters breaking time-reversal symmetry: $(\cos k_x - \cos k_y) \tau_z \sigma_x$, $\sin k_x \sin k_y \tau_0 \sigma_x$, $\sin k_x \sin k_y \tau_z \sigma_y$, $\sin k_y \sin k_z \tau_0 \sigma_z$, $\cos \frac{k_x}{2} \sin \frac{k_y}{2} \sin \frac{k_z}{2} \tau_x \sigma_z$, $\sin k_x \sin k_z \tau_z \sigma_z$, $\sin k_y \sin k_z (\cos k_x - \cos k_y) \tau_0 \sigma_z$, $\sin k_x \sin k_z (\cos k_x - \cos k_y) \tau_z \sigma_z$, $(\cos k_x - \cos k_y) \tau_z \sigma_x$, $(\cos k_x - \cos k_y) \tau_0 \sigma_y$, and $\cos \frac{k_x}{2} \sin \frac{k_y}{2} \sin \frac{k_z}{2} \tau_y$. Remarkably, the last one corresponds to a pure orbital current state that couples to the Néel order, but there are other orders with different spin textures.

In Table S2, we include the SOC dependence of the Landau coefficients for each of the previous secondary order parameters, considering the bilinear coupling to both N_x and M_y , obtained by evaluating the one-loop diagram in Fig. S1(a). For instance, Table S2 shows that $(\cos k_x - \cos k_y) \tau_z \sigma_x$ is able to couple to $\tau_z \sigma_x$ with a coefficient quadratic in SOC and it also couples to $\tau_0 \sigma_y$ with a coefficient linear in SOC. Among all secondary order parameters, quadratic SOC dependence of the FM spin moment (which is obtained by adding $n_{FM,O}$ and $n_{AM,O}$) can be obtained through 4 secondary order parameters: $\sin k_x \sin k_y \tau_0 \sigma_x$, $\sin k_x \sin k_y \tau_z \sigma_y$, $\cos \frac{k_x}{2} \sin \frac{k_y}{2} \sin \frac{k_z}{2} \tau_x \sigma_z$, and $\cos \frac{k_x}{2} \sin \frac{k_y}{2} \sin \frac{k_z}{2} \tau_y$. Other secondary order parameters lead to cubic SOC dependence of the FM spin moment.

Table S2. SOC dependence of the Landau coefficients for the bilinear coupling between secondary order parameters \hat{O} and N_x and M_y , calculated from the one-loop diagram in Fig. S1(a). Space group D_{4h} with site symmetry B_{2g} ($k_x k_y$) is considered. Here, coefficients $c_{AM,O}$ for $N_x \hat{O}$ has SOC dependence $c_{AM,O} \propto \lambda^{n_{AM,O}}$, and coefficients $c_{FM,O}$ for $M_y \hat{O}$ has SOC dependence $c_{FM,O} \propto \lambda^{n_{FM,O}}$. A cross denotes that the coefficient vanishes at 1-loop level, and thus the leading SOC dependence between N_x and M_y is quadratic.

\hat{O}	$n_{AM,O}$	$n_{FM,O}$
$\tau_z \sigma_x$	0	\times
$\sin k_x \sin k_y \sigma_x$	0	2
$\sin \frac{k_x}{2} \sin \frac{k_y}{2} \tau_x \sigma_x$	0	\times
$\tau_x \sigma_y$	\times	0
$\sin k_x \sin k_y \tau_z \sigma_y$	2	0
$\sin k_y \sin k_z \sigma_z$	1	2
$\cos \frac{k_x}{2} \sin \frac{k_y}{2} \sin k_z \tau_x \sigma_z$	1	1
$\sin k_x \sin k_z \tau_z \sigma_z$	2	1
$\cos \frac{k_x}{2} \sin \frac{k_y}{2} \sin k_z \tau_y$	1	1
$\tau_z \sigma_x$	0	\times
σ_y	\times	0

\hat{O}	$n_{AM,O}$	$n_{FM,O}$
$(\cos k_x - \cos k_y) \tau_z \sigma_x$	2	1
$\sin k_x \sin k_y (\cos k_x - \cos k_y) \sigma_x$	\times	\times
$\sin \frac{k_x}{2} \sin \frac{k_y}{2} (\cos k_x - \cos k_y) \tau_x \sigma_x$	\times	1
$(\cos k_x - \cos k_y) \tau_x \sigma_y$	1	\times
$\sin k_x \sin k_y (\cos k_x - \cos k_y) \tau_z \sigma_y$	\times	\times
$\sin k_y \sin k_z (\cos k_x - \cos k_y) \sigma_z$	1	2
$\cos \frac{k_x}{2} \sin \frac{k_y}{2} \sin k_z (\cos k_x - \cos k_y) \tau_x \sigma_z$	1	\times
$\sin k_x \sin k_z (\cos k_x - \cos k_y) \tau_z \sigma_z$	2	1
$\cos \frac{k_x}{2} \sin \frac{k_y}{2} \sin k_z (\cos k_x - \cos k_y) \tau_y$	\times	1
$(\cos k_x - \cos k_y) \tau_z \sigma_x$	2	1
$(\cos k_x - \cos k_y) \sigma_y$	1	2

Table S3. Tight-binding hoppings and SOC entering in the minimal model in Eq. (2) of the main text relevant for the rutile lattice and FeSb₂, as identified in Ref. [3]. The hopping and SOC parameters are detailed in Table S4.

	Rutile lattice			FeSb ₂		
$t_{x,\mathbf{k}}$	$t_8 \cos \frac{k_x}{2} \cos \frac{k_y}{2} \cos \frac{k_z}{2}$					
$t_{z,\mathbf{k}}$	$t_6 \sin k_x \sin k_y + t_7 \sin k_x \sin k_y \cos k_z$					
$\lambda_{x,\mathbf{k}}$	$\lambda \sin \frac{k_z}{2} \sin \frac{k_x}{2} \cos \frac{k_y}{2}$			$\lambda_x \sin \frac{k_z}{2} \sin \frac{k_x}{2} \cos \frac{k_y}{2}$		
$\lambda_{y,\mathbf{k}}$	$-\lambda \sin \frac{k_z}{2} \sin \frac{k_y}{2} \cos \frac{k_x}{2}$			$\lambda_y \sin \frac{k_z}{2} \sin \frac{k_y}{2} \cos \frac{k_x}{2}$		
$\lambda_{z,\mathbf{k}}$	$\lambda_z \cos \frac{k_z}{2} \cos \frac{k_x}{2} \cos \frac{k_y}{2} (\cos k_x - \cos k_y)$			$\lambda_z \cos \frac{k_z}{2} \cos \frac{k_x}{2} \cos \frac{k_y}{2}$		
$\varepsilon_{0,\mathbf{k}}$	$t_1(\cos k_x + \cos k_y) + t_2 \cos k_z + t_3 \cos k_x \cos k_y + t_4(\cos k_x + \cos k_y) \cos k_z + t_5 \cos k_x \cos k_y \cos k_z - \mu$			$t_{1,x} \cos k_x + t_{1,y} \cos k_y + t_2 \cos k_z + t_3 \cos k_x \cos k_y + t_{4,x} \cos k_x \cos k_z + t_{4,y} \cos k_y \cos k_z + t_5 \cos k_x \cos k_y \cos k_z - \mu$		

Table S4. Tight-binding hopping parameters in units of eV found in Ref. [3] used to obtain the band structures in Fig. (1) of the main text and Figs. S4-S5. The SOC parameters estimated from DFT results.

RuO ₂	t_1	t_2	t_3	t_4	t_5	t_6	t_7	t_8	μ	λ	λ_z
	-0.05	0.7	0.5	-0.15	-0.4	-0.6	0.3	1.7	0.25	0.05	0.17
FeSb ₂	$t_{1,x}$	$t_{1,y}$	t_2	t_3	$t_{4,x}$	$t_{4,y}$	t_5	t_6	t_7	t_8	μ
	-0.1	-0.05	-0.05	0.06	0.1	0.05	-0.05	0.05	-0.1	0.15	-0.12
										λ_x	λ_y
											λ_z
										0.0027	0.0066
											0.075

S5. HOPPING PARAMETERS AND SOC FOR THE RUTILE LATTICE AND FeSb₂

The general form for the normal-state Hamiltonian describing altermagnetism is given in Eq. (2) of the main text. In Tables S3 - S4 we detail the relevant form for the hoppings and spin-orbit coupling for the rutile lattice (SG 136) and FeSb₂ (SG 58) used to obtain the band structures and the magnetizations as a function of the SOC strength shown in Fig. (2) of the main text.

In order to estimate the SOC for FeSb₂, we perform DFT calculations using Wien2k [4] (SG 58, $a = 5.8379\text{\AA}$, $b = 6.5248\text{\AA}$, $c = 3.1811\text{\AA}$, internal position $(x, y, z) = (0.20094827, 0.35723599, 0)$ for Sb on Wyckoff position 4g), and read off the splittings induced by the spin-orbit terms at $\mathbf{k}_1 = (\pi, 0, \pi)$ where $t_{x,\mathbf{k}_1} = t_{z,\mathbf{k}_1} = \lambda_{y,\mathbf{k}_1} = \lambda_{z,\mathbf{k}_1} = 0$ and the splitting is solely induced by $\lambda_{x,\mathbf{k}_1} = \lambda_x$. Similarly, at $\mathbf{k}_2 = (0, \pi, \pi)$, we have $t_{x,\mathbf{k}_2} = t_{z,\mathbf{k}_2} = \lambda_{x,\mathbf{k}_2} = \lambda_{z,\mathbf{k}_2} = 0$ and the splitting is given by $\lambda_{y,\mathbf{k}_2} = \lambda_y$. Finally, for λ_z we use the self-consistently converged densities in the DFT calculation with SOC, but calculate the eigenenergies without including the SOC perturbatively. The energy shift ΔE of the band positions with and without SOC at the Γ point is given by $\Delta E = \sqrt{t_8^2 + \lambda_z^2} - |t_8|$ since the other components of the SOC vanish. Using that $t_8 = 0.15$ eV, we obtain $\vec{\lambda}_0 = (2.7, 6.6, 75)$ meV as used for the calculations in the main text.

For RuO₂, we use the same procedure, i.e. a DFT calculation using Wien2k [4] (SG 136, $a = 4.4825\text{\AA}$, $c = 3.1113\text{\AA}$, internal position $(x, y, z) = (0.30544216, 0.30544216, 0)$ for O on Wyckoff position 4f, and Ru on Wyckoff position 2a), once with spin-orbit coupling and once without it. We then find λ at the point $\mathbf{k}_3 = (\pi, 0, \pi)$ where all but $\lambda_{x,\mathbf{k}}$ vanish. λ_z is here identified at the point $\mathbf{k}_4 = (\frac{\pi}{2}, 0, 0)$ where $\Delta E = \frac{1}{\sqrt{2}}(\sqrt{t_8^2 + \lambda_z^2} - |t_8|)$. For RuO₂ we then obtain $\vec{\lambda}_0 = (0.05, 0.05, 0.17)$ eV.

S6. GENERAL EXPRESSIONS FOR THE BERRY CURVATURE

In the presence of SOC, the Néel order \vec{N} induces a FM order \vec{M} . Focusing on the previous cases of the rutile lattice and FeSb₂, the free energy invariant corresponds to $M_x N_y + M_y N_x$. Therefore, an in-plane Néel order $\vec{N} = (N_x, 0, 0)$ induces a magnetization $\vec{M} = (0, M_y, 0)$. In the presence of these orders, the Hamiltonian without including the dispersion corresponds to

$$H = t_{x,\mathbf{k}} \tau_x + t_{z,\mathbf{k}} \tau_z + \tau_y \vec{\lambda}_{\mathbf{k}} \cdot \vec{\sigma} + M_y \sigma_y + N_x \tau_z \sigma_x, \quad (\text{S15})$$

with

$$E_{\alpha=\pm, \beta=\pm} = \alpha \left(N_x^2 + M_y^2 + \vec{\lambda}_{\mathbf{k}}^2 + t_{x,\mathbf{k}}^2 + t_{z,\mathbf{k}}^2 + \beta 2 \sqrt{N_x^2 (\lambda_{z,\mathbf{k}}^2 + \lambda_{y,\mathbf{k}}^2 + t_{z,\mathbf{k}}^2) + M_y^2 (\lambda_{y,\mathbf{k}}^2 + t_{z,\mathbf{k}}^2 + t_{x,\mathbf{k}}^2)} - 2N_x M_y \lambda_{z,\mathbf{k}} t_{x,\mathbf{k}} \right)^{1/2}. \quad (\text{S16})$$

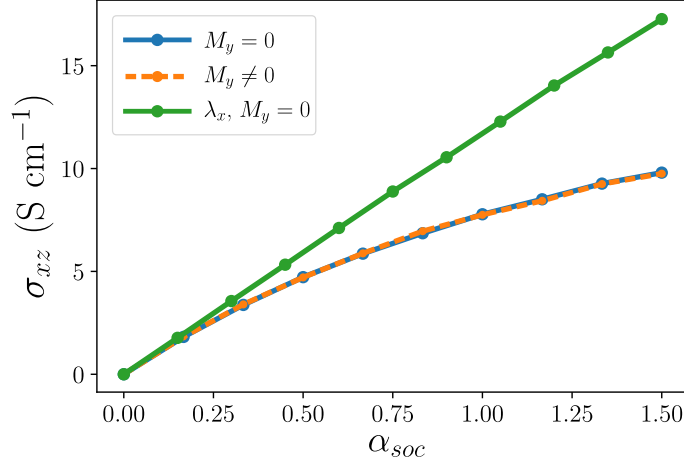


Figure S2. Hall conductivity as a function of SOC strength for RuO₂, considering the tight-binding model and parameters in Tables S3-S4. We take $\vec{\lambda} = \alpha_{soc}\vec{\lambda}_0$ with $\vec{\lambda}_0 = (0.05, 0.05, 0.17)$ eV and $N_x = 0.2$ eV. The orange (blue) line corresponds to the Berry curvature in Eq. (S17) (Eq. (S19)). The green line is obtained from the Berry curvature in Eq. (S19) considering only SOC in the x -direction.

The general lowest-order expression for the Berry curvature is given by [2]

$$\Omega_{\alpha,\beta,ij} = \sum_{m,n=i,j} \varepsilon_{mn} \left[\frac{3M_y}{8E_2} \left(\frac{\beta(N_x^2 + M_y^2)}{3E_2^2} + \frac{\beta N_x^2(N_x^2 + t_{x,\mathbf{k}}^2 + 2M_y^2) + \beta M_y^4}{E_{\alpha\beta}^2 E_2^2} + \frac{2(N_x^2 + M_y^2)}{E_{\alpha\beta}^2 E_2} + \frac{\beta}{E_{\alpha\beta}^2} \right) \right. \\ \times (\lambda_{y,\mathbf{k}} \partial_m t_{x,\mathbf{k}} \partial_n t_{z,\mathbf{k}} + t_{x,\mathbf{k}} \partial_m t_{z,\mathbf{k}} \partial_n \lambda_{y,\mathbf{k}} + t_{z,\mathbf{k}} \partial_m \lambda_{y,\mathbf{k}} \partial_n t_{x,\mathbf{k}}) \\ + \frac{N_x t_{z,\mathbf{k}}}{8E_{\alpha\beta}^3} \left(\frac{\beta(N_x^2 t_{z,\mathbf{k}}^2 + M_y^2(t_{x,\mathbf{k}}^2 + t_{z,\mathbf{k}}^2))}{E_2^3} + \frac{3\beta}{E_2} \right) (\lambda_{x,\mathbf{k}} \partial_m t_{x,\mathbf{k}} \partial_n t_{z,\mathbf{k}} + t_{x,\mathbf{k}} \partial_m t_{z,\mathbf{k}} \partial_n \lambda_{x,\mathbf{k}} + t_{z,\mathbf{k}} \partial_m \lambda_{x,\mathbf{k}} \partial_n t_{x,\mathbf{k}}) \\ \left. + \frac{N_x}{8E_{\alpha\beta}^3} \left(\frac{3N_x^2 t_{z,\mathbf{k}}^2 + 3M_y^2(t_{x,\mathbf{k}}^2 + t_{z,\mathbf{k}}^2)}{E_2^2} + 1 \right) (\partial_m \lambda_{x,\mathbf{k}} \partial_n t_{x,\mathbf{k}}) \right], \quad (S17)$$

where we introduced

$$E_2 = \sqrt{N_x^2 (\lambda_{z,\mathbf{k}}^2 + \lambda_{y,\mathbf{k}}^2 + t_{z,\mathbf{k}}^2) + M_y^2 (\lambda_{y,\mathbf{k}}^2 + t_{z,\mathbf{k}}^2 + t_{x,\mathbf{k}}^2)} - 2N_x M_y \lambda_{z,\mathbf{k}} t_{x,\mathbf{k}}, \quad (S18)$$

which has units of energy squared. When $M_y = 0$, Eq. (S17) reduces to

$$\Omega_{\alpha,\beta,ij} = \frac{1}{8E_{\alpha\beta}^3} \sum_{m,n=i,j} \varepsilon_{mn} \left[\left(N_x + \frac{3N_x t_{z,\mathbf{k}}^2}{E_1^2} + \frac{3\beta t_{z,\mathbf{k}}^2}{E_1} + \frac{\beta t_{z,\mathbf{k}}^4}{E_1^3} \right) \partial_m \lambda_{x,\mathbf{k}} \partial_n t_{x,\mathbf{k}} + \left(\frac{3\beta \lambda_{x,\mathbf{k}} t_{z,\mathbf{k}}}{E_1} + \frac{\beta \lambda_{x,\mathbf{k}} t_{z,\mathbf{k}}^3}{E_1^3} \right) \partial_m t_{x,\mathbf{k}} \partial_n t_{z,\mathbf{k}} \right. \\ \left. + \left(\frac{3\beta t_{x,\mathbf{k}} t_{z,\mathbf{k}}}{E_1} + \frac{\beta t_{x,\mathbf{k}} t_{z,\mathbf{k}}^3}{E_1^3} \right) \partial_m t_{z,\mathbf{k}} \partial_n \lambda_{x,\mathbf{k}} \right], \quad (S19)$$

which includes SOC components in all direction and where now $E_1 = \sqrt{t_{z,\mathbf{k}}^2 + \lambda_{z,\mathbf{k}}^2 + \lambda_{y,\mathbf{k}}^2}$. For $\lambda_{y,\mathbf{k}} = \lambda_{z,\mathbf{k}} = 0$, this expression further reduces to Eq. (10) in the main text.

We have additionally considered the Berry curvature in the presence of only an in-plane M_y magnetization. In this case, Eq. (S17) reduces to

$$\Omega_{\alpha,\beta,ij}^{(M_y)} = \frac{\text{sgn}(M_y)\beta}{8\tilde{E}_y^3} \sum_{m,n=i,j} \varepsilon_{mn} \left[\left(1 + \frac{3}{E_{\alpha\beta}^2} (\tilde{E}_y + \beta|M_y|)^2 \right) (t_{z,\mathbf{k}} \partial_m \lambda_{y,\mathbf{k}} \partial_n t_{x,\mathbf{k}} + t_{x,\mathbf{k}} \partial_m t_{z,\mathbf{k}} \partial_n \lambda_{y,\mathbf{k}} + \lambda_{y,\mathbf{k}} \partial_m t_{x,\mathbf{k}} \partial_n t_{z,\mathbf{k}}) \right], \quad (S20)$$

and the Berry curvature is also linear in the SOC component parallel to the magnetization. In the previous expression, $\tilde{E}_y = \sqrt{t_{z,\mathbf{k}}^2 + t_{x,\mathbf{k}}^2 + \lambda_{y,\mathbf{k}}^2}$ and $E_{\alpha=\pm, \beta=\pm}$ is now Eq. (S16) in the case $N_x = 0$. The dispersion of the spin up and spin down bands is different in the presence of \vec{M} , and consequently this term also give rise to a finite AHE.

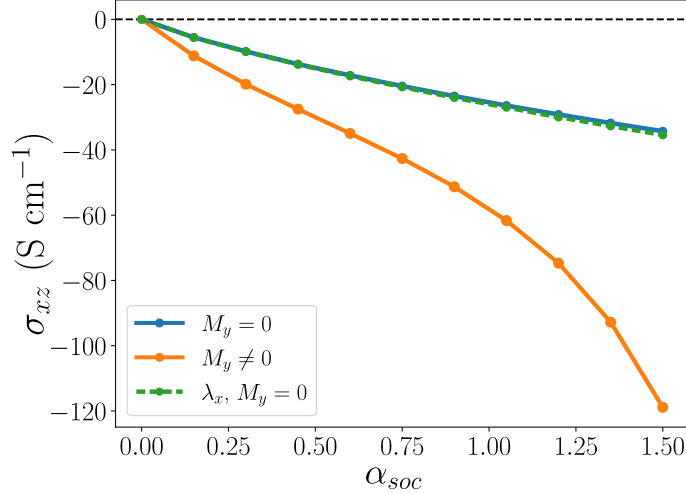


Figure S3. Hall conductivity as a function of SOC strength for FeSb₂, considering the tight-binding model and parameters in Tables S3-S4. We take $\vec{\lambda} = \alpha_{soc}\vec{\lambda}_0$ with $\vec{\lambda}_0 = (0.0027, 0.0066, 0.075)$ eV and $N_x = 0.05$ eV. The orange (blue) line corresponds to the Berry curvature in Eq. (S17) (Eq. (S19)). The green line is obtained from the Berry curvature in Eq. (S19) considering only SOC in the x -direction.

In Figs. S2-S3 we show the Hall conductivity for the rutile lattice and the FeSb₂ tight-binding models (see Tables S3-S4), calculated from the Berry curvature as

$$\sigma_{ij} = -\frac{e^2}{\hbar} \int_{BZ} \frac{d\mathbf{k}}{(2\pi)^3} \sum_{\alpha, \beta} f_{\alpha, \beta}(\mathbf{k}) \Omega_{\alpha, \beta, ij}, \quad (S21)$$

where $f_{\alpha, \beta}(\mathbf{k})$ is the Fermi-Dirac contribution of each band α, β . In the case of RuO₂ ($P = D_{4h}$, $\Gamma_N = B_{2g}$), see Fig. S2, Eqs. (S17) and (S19) yield almost the same result for the conductivity. Therefore, the induced magnetization for this tetragonal material does not give rise to a significant contribution to the anomalous Hall conductivity, as expected from Table I in the main text, since \vec{M} is induced to second (or higher order) in the SOC. In contrast, if we focus on the band structure inspired by FeSb₂ ($P = D_{2h}$, $\Gamma_N = B_{1g}$), the induced magnetization \vec{M} is allowed to linear order in SOC (see Table I in the main text) and may give rise to significant contributions to the anomalous Hall conductivity, as seen from Fig. S3.

S7. MAGNETIC ANISOTROPY ENERGY

In this section, we derive the expression for the magnetic anisotropy energy and examine the preferred direction using microscopic models relevant for the rutile lattice (SG 136) and FeSb₂ (SG 58). In the presence of the Néel order parameter and SOC the free energy is given by

$$F = s_x N_x^2 + s_y N_y^2 + s_z N_z^2. \quad (S22)$$

In Eq. (1) of the main text we rewrite this expression in the form

$$F = s_0(N_x^2 + N_y^2 + N_z^2) + s_1(N_x^2 - N_y^2) + s_2(N_x^2 + N_y^2 - 2N_z^2), \quad (S23)$$

so that the coefficients s_0 , s_1 and s_2 correspond to

$$\begin{aligned} s_0 &= \frac{1}{3}(s_x + s_y + s_z), \\ s_1 &= \frac{1}{2}(s_x - s_y), \\ s_2 &= \frac{1}{6}(s_x + s_y - 2s_z). \end{aligned} \quad (S24)$$

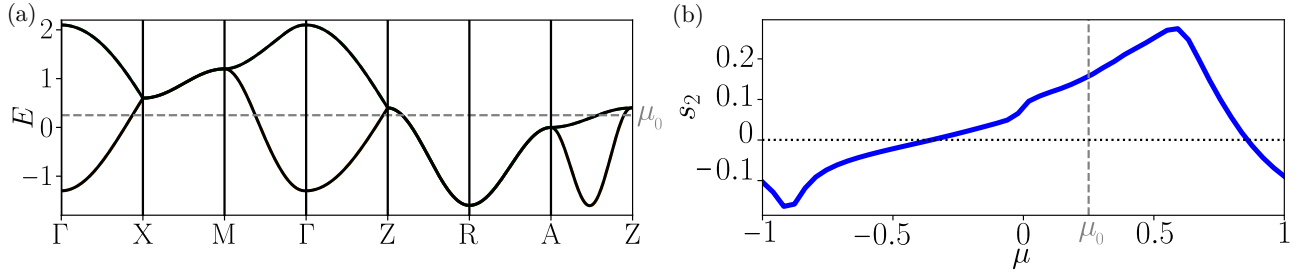


Figure S4. (a) Normal state band structure relevant for the rutile lattice (SG 136), using the tight-binding model in Table S3 and considering the hopping parameters in Table S4. (b) s_2 coefficient (see Eqs. (S23), (S28)) as a function of the chemical potential μ for the band structure shown in (a) and taking $T = 0.02$, $n_{\mathbf{k}} = 201^3$ and the SOC terms in Tables S3 - S4, displaying that the preferred direction for the Néel vector can switch by varying the Fermi energy.

The expression for the coefficients is derived from the following contribution of the free energy to second order (see Fig. S1(a)),

$$F_J^{(2)} = \frac{1}{2\beta} \sum_{i\omega_n} \text{Tr} \left[\sum_{a,b} G^a(\mathbf{k}, i\omega_n) G^b(\mathbf{k}, i\omega_n) \tau_z \vec{N} \cdot \vec{\sigma} P_{\mathbf{k}}^a \tau_z \vec{N} \cdot \vec{\sigma} P_{\mathbf{k}}^b \right], \quad (\text{S25})$$

where $G^a(\mathbf{k}, i\omega_n)$ and $P_{\mathbf{k}}^a$ are the Green's function and the projector operator defined in Eq. (S7) and Eq. (S8), respectively. In particular, we are concerned with the corrections due to SOC, and therefore we specifically analyze the trace

$$\begin{aligned} & \frac{1}{16} \text{Tr} \left[\tau_z \vec{N} \cdot \vec{\sigma} \tau_y \lambda_{\mathbf{k}} \cdot \vec{\sigma} \tau_z \vec{N} \cdot \vec{\sigma} \tau_y \lambda_{\mathbf{k}} \cdot \vec{\sigma} \right] \\ &= -\frac{1}{4} \left\{ N_x^2 (\lambda_{x,\mathbf{k}}^2 - \lambda_{y,\mathbf{k}}^2 - \lambda_{z,\mathbf{k}}^2) + N_y^2 (-\lambda_{x,\mathbf{k}}^2 + \lambda_{y,\mathbf{k}}^2 - \lambda_{z,\mathbf{k}}^2) + N_z^2 (-\lambda_{x,\mathbf{k}}^2 - \lambda_{y,\mathbf{k}}^2 + \lambda_{z,\mathbf{k}}^2) \right. \\ & \quad \left. + 4(N_x N_y \lambda_{x,\mathbf{k}} \lambda_{y,\mathbf{k}} + N_x N_z \lambda_{x,\mathbf{k}} \lambda_{z,\mathbf{k}} + N_y N_z \lambda_{y,\mathbf{k}} \lambda_{z,\mathbf{k}}) \right\}. \end{aligned} \quad (\text{S26})$$

From this expression, the general form of the free energy in Eq. (S1) directly follows. Focusing on orthorhombic or higher-symmetry groups, the form for the s_x , s_y and s_z coefficients in Eq. (S22) corresponds to

$$s_{i=\{x,y,z\}} = a_N - \sum_{\mathbf{k}} \frac{L(\mathbf{k})}{2\tilde{E}_{\mathbf{k}}^2} (\lambda_{i,\mathbf{k}}^2 - \sum_{j \neq i} \lambda_{j,\mathbf{k}}^2), \quad (\text{S27})$$

where the function $L(\mathbf{k})$ is defined in Eq. (8) of the main text. Thus, replacing this result in Eq. (S24),

$$\begin{aligned} s_0 &= a_N + \frac{1}{6} \sum_{\mathbf{k}} \frac{\lambda_{x,\mathbf{k}}^2 + \lambda_{y,\mathbf{k}}^2 + \lambda_{z,\mathbf{k}}^2}{\tilde{E}_{\mathbf{k}}^2} L(\mathbf{k}), \\ s_1 &= -\frac{1}{2} \sum_{\mathbf{k}} \frac{\lambda_{x,\mathbf{k}}^2 - \lambda_{y,\mathbf{k}}^2}{\tilde{E}_{\mathbf{k}}^2} L(\mathbf{k}), \\ s_2 &= -\frac{1}{6} \sum_{\mathbf{k}} \frac{\lambda_{x,\mathbf{k}}^2 + \lambda_{y,\mathbf{k}}^2 - 2\lambda_{z,\mathbf{k}}^2}{\tilde{E}_{\mathbf{k}}^2} L(\mathbf{k}). \end{aligned} \quad (\text{S28})$$

In Fig. S4 and S5 we show the magnetic anisotropy coefficients for two different tight binding models. First, we focus on a model relevant for the rutile lattice (SG 136) with the band structure shown in Fig. S4(a). In this tetragonal case, the coefficient s_1 vanishes by symmetry, and s_2 determines the in-plane versus out-of-plane spin anisotropy. As seen from Fig. S4(b), for the chemical potential μ_0 the preferred direction for the Néel vector is out-of-plane. However, for a lower μ it changes to in-plane, which may be due to the competition between the Linhard function and the density of states in the function $L(\mathbf{k})$. Considering now the tight-binding model inspired by the FeSb₂ band structure, see Fig. S5(a), for this orthorhombic material both coefficients s_1 and s_2 are generally non-zero. For the chemical

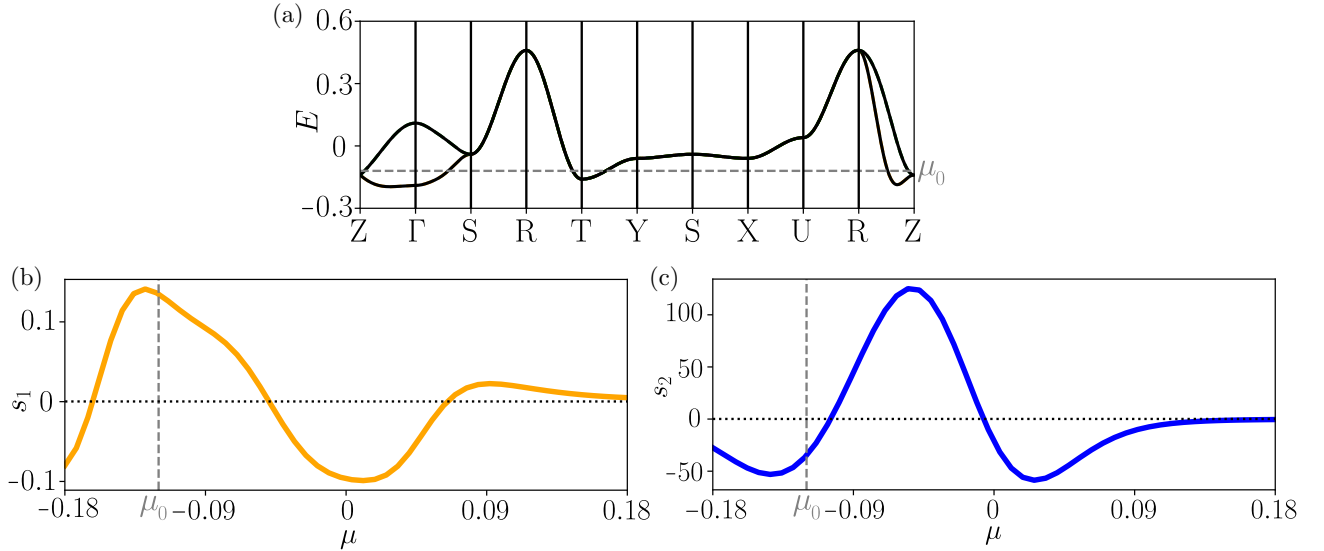


Figure S5. (a) Normal state band structure relevant for the FeSb₂ lattice (SG 58), using the tight-binding model in Table S3 and considering the hopping parameters in Table S4. (b)-(c) s_1 and s_2 coefficients (see Eqs. (S23), (S28)) as a function of μ for the band structure shown in (a) and taking $T = 0.02$, $n_{\mathbf{k}} = 201^3$ and the SOC terms in Tables S3 - S4, displaying that both the in-plane and out-of-plane preferred direction for the Néel vector can switch by varying the Fermi energy.

potential μ_0 , Figs. S5(b)-(c) show that the preferred direction of the altermagnetic moments is along the y direction, but similar to the rutile case it can switch as a function of the Fermi energy.

[1] Matthias Hecker, Anant Rastogi, Daniel F. Agterberg, and Rafael M. Fernandes, “Classification of electronic nematicity in three-dimensional crystals and quasicrystals,” Phys. Rev. B **109**, 235148 (2024).
[2] Ansgar Graf and Frédéric Piéchon, “Berry curvature and quantum metric in N -band systems: An eigenprojector approach,” Phys. Rev. B **104**, 085114 (2021).
[3] Mercè Roig, Andreas Kreisel, Yue Yu, Brian M. Andersen, and Daniel F. Agterberg, “Minimal models for altermagnetism,” Phys. Rev. B **110**, 144412 (2024).
[4] P. Blaha, K. Schwarz, G. K. Madsen, D. Kvasnicka, and J. Luitz, *WIEN2k an Augmented Plane Wave Plus Local Orbitals Program for Calculating Crystal Properties* (Technische Universität Wien, 2001).